Title

Magnetisation transfer, diffusion and g-ratio measures of demyelination and neurodegeneration in early relapsing-remitting multiple sclerosis: a longitudinal microstructural MRI study

Author names and affiliations

Elizabeth N. York[1,2,3], Rozanna Meijboom[1,2], Michael J. Thrippleton[1,2], Mark E. Bastin,[1,2] Agniete Kampaite,[1,2] Nicole White,[1,2] Siddharthan Chandran,[1,3,4] Adam D. Waldman[1,2]; on behalf of the Future-MS Consortium.

[1]Centre for Clinical Brain Sciences, University of Edinburgh, Edinburgh, United Kingdom

[2]Edinburgh Imaging, University of Edinburgh, Edinburgh, United Kingdom

[3]Anne Rowling Regenerative Neurology Clinic, Edinburgh, United Kingdom

[4]UK Dementia Research Institute, University of Edinburgh, Edinburgh, United Kingdom

Correspondence:

Elizabeth N. York eyork@ed.ac.uk

Adam D Waldman adam.waldman@ed.ac.uk
Centre for Clinical Brain Sciences, University of Edinburgh
Edinburgh BioQuarter: Chancellors Building
Edinburgh EH16 4SB, United Kingdom
Tel: 0131 242 6200

Abstract

Introduction

Relapsing-remitting multiple sclerosis (RRMS) is a chronic, immune-mediated neurodegenerative disease with a highly heterogeneous disease course. Conventional MRI is widely used for diagnosis and disease monitoring but provides limited specific information on MS-related damage. Improved *in vivo* biomarkers, which are sensitive to subtle changes in RRMS pathology, are needed for early patient stratification and evaluation of neuroprotective and disease modifying therapies (DMTs).

Quantitative MRI methods, such as myelin-sensitive magnetisation transfer ratio (MTR) or saturation (MTsat) imaging, axon-sensitive diffusion Neurite Orientation Dispersion and Density Imaging (NODDI) and derived aggregate measures (e.g. MR g-ratio) may provide more specific indices of microstructural damage in RRMS.

The aim of this study was to determine the sensitivity of microstructural MRI markers (magnetisation transfer ratio [MTR], MTsat, NODDI isotropic/intraneurite volume fractions, and g-ratio) to myelin and axonal damage in white matter lesions (WML) and normal appearing white matter (NAWM) and their longitudinal change in early RRMS.

Methods

Seventy-seven people were recruited to an extended MRI sub-study of Future-MS, a longitudinal study of people with recently diagnosed RRMS. MR imaging and clinical assessment were performed at baseline, prior to initiation of any DMTs, and one year later. Twelve healthy volunteers additionally received the same MR protocol, repeated within two weeks, to determine test-retest agreement. Approval was granted from the local Research Ethics committee and participants provided written informed consent.

A 3T MR imaging protocol included structural 3D T1-weighted and T2-weighted FLAIR sequences, magnetisation transfer acquisition (comprising two proton density images with and without a saturation pulse, plus a T1-weighted image), and multishell diffusion-weighted 2D echo-planar imaging.

MTR and MTsat were calculated from magnetisation transfer data, and NODDI isotropic and intraneurite volume fractions (ISOVF and ICVF, respectively) from diffusion-weighted data. The g-ratio was calculated from MTsat and NODDI data. WML and NAWM tissue masks were segmented from structural images.

Tissue contrast for MTsat and MTR was compared with paired t-tests. Voxelwise distributions of microstructural metrics were examined graphically.

Longitudinal change in MR-derived measures in NAWM and WML was assessed with paired t-tests (α=0.05) with follow-up linear mixed models, where significant, to control for confounding factors, with False Discovery Rate (FDR) correction for multiple comparisons.

Results

Complete longitudinal data for MTsat and MTR was available for sixty-two patients, and sixty patients for NODDI and g-ratio.

Contrast between NAWM and WML was greater for MTsat than MTR (mean difference = 16.9 [95% CI 15.96 to 17.89], paired t-test: $t(74)=34.97$, $p<0.001$). Voxelwise histograms showed a negative linear dependence on the approximation of T1 recovery (T1app) for MTsat, but not MTR, in NAWM and a non-linear association in WML.

Simulations and voxelwise histograms demonstrated that g-ratio is inversely related to MTsat and NODDI ISOVF but positively related to NODDI ICVF. MTsat and NODDI ICVF were not associated in control white matter or NAWM but broadly co-correlated in WML.

In NAWM, g-ratio and NODDI ICVF increased significantly over one year (mean difference = 0.004 [95% CI 0.001 to 0.007] and 0.002 [0.0002 to 0.004], paired t-test: $t(59) = 2.60$ and 2.29, $p = 0.012$ and 0.025 respectively) and MTsat decreased (mean difference = -0.032 [95% CI -0.061 to -0.003], $t(61) = -2.19$, $p = 0.033$). Neither MTR nor NODDI ISOVF changed significantly over one year ($p=0.94$ and $p=0.67$).

After accounting for covariates and adjustment for multiple comparisons, the longitudinal increase in g-ratio and in NODDI ICVF remained significant (linear mixed

model: adjusted mean difference = 0.007 and 0.004, t(75.9) = 3.08 and t(90.6) = 3.51, FDR-corrected p = 0.029 and 0.007). The decrease in MTsat did not survive correction for multiple comparisons (FDR-corrected p = 0.11).

In WML, paired t-tests revealed increases in MTsat, MTR, NODDI ISOVF and ICVF over one year, but no change in g-ratio. Follow-up linear mixed models, however, showed that only changes in MTsat and NODDI metrics were significant after correction for confounding factors and multiple comparisons.

Longitudinal change did not, however, generally exceed healthy control test-retest limits of agreement except for NODDI ISOVF and ICVF in WML.

Discussion

Higher tissue contrast for MTsat compared with MTR suggests MTsat is more sensitive to demyelination than widely used MTR. Comparisons of microstructural MRI data distributions indicate that MTsat is better suited to measurement of subtle myelin loss in NAWM compared with MTR.

NAWM data distributions suggest that MTsat and NODDI ICVF provide independent measures of myelin and axonal integrity. Simulations show that g-ratio increases as MTsat decreases, but changes in NODDI parameters may complicate interpretation of longitudinal change in g-ratio.

The observed increase in g-ratio and MTsat in NAWM is indicative of subtle myelin loss in patients with early RRMS. The unexpected increase observed in NODDI ICVF suggests axonal swelling and/or axonal repair, and may confound g-ratio.

Increases in MTsat and NODDI ICVF in WML are also suggestive of tissue repair. WML g-ratio did not change over time, likely due to competing effects of longitudinal MTsat and NODDI changes.

Despite significant groupwise effects, detection of longitudinal change at an individual level may be limited by technique test-retest agreement in early RRMS.

Conclusion

MTsat and g-ratio are promising *in vivo* biomarkers of myelin integrity in early RRMS, and appear more sensitive than MTR for detecting subtle demyelination. Our findings suggest that MTsat and g-ratio measures may be most sensitive for

detecting subtle change in NAWM, as compared with more severely damaged WML where T1 effects and neuroaxonal damage predominate. Complex dependence of g-ratio on NODDI parameters illustrates the limitation of interpreting such aggregate measures in isolation, and independent consideration of myelin-sensitive and axonal neuroimaging markers may ultimately be more informative for longitudinal tracking of neuropathology in RRMS. Technique reproducibility currently limits evaluation in individual patients, and future research is warranted to validate diffusion and MT models across heterogeneous microstructural damage found in MS, for translation into clinical practice and trial platforms.

Keywords

Magnetisation transfer imaging; MTsat; g-ratio; NODDI; diffusion-weighted imaging; multiple sclerosis.

Abbreviations

CNR	Contrast-to-noise ratio
CNS	Central nervous system
dMRI	Diffusion-weighted magnetic resonance imaging
DMTs	Disease-modifying therapies
EDSS	Expanded Disability Status Scale
ICVF	(NODDI-derived) intraneurite signal fraction
ihMTR	Inhomogeneous magnetisation transfer ratio
ISOVF	(NODDI-derived) isotropic signal fraction
MR	Magnetic resonance
MS	Multiple sclerosis
MSFC	Multiple Sclerosis Functional Composite
MTI	Magnetisation transfer imaging
MTR	Magnetisation transfer ratio
MTsat	Magnetisation transfer saturation
NAWM	‘Normal-appearing’ white matter
NODDI	Neurite Orientation Dispersion and Density Imaging
ODI	(NODDI-derived) orientation dispersion index
RRMS	Relapsing-remitting multiple sclerosis
SNR	Signal-to-noise
SPMS	Secondary progressive multiple sclerosis
WML	White matter lesions

Introduction

Multiple sclerosis and the need for longitudinal biomarkers

Multiple sclerosis (MS) is a chronic, immune-mediated, neurodegenerative disease.[1,2] Neuroinflammation and widespread focal injury to myelin (*lesions*) within the central nervous system (CNS) may result in irreversible neurodegeneration for people with MS.[3-5]

Clinical symptomology (e.g. motor impairment, fatigue, visual disturbances) and the MS disease course are heterogeneous.[6-8] People with relapsing-remitting MS (RRMS) experience relapses interspersed with periods of remission; secondary progressive MS (SPMS) begins with a relapsing-remitting pattern but clinical disability later becomes progressive, without periods of remission.[9]

Disease-modifying therapies (DMTs), which typically modulate neuroinflammation, reduce the number of relapses and may lower the risk of converting to SPMS.[10] It is difficult to predict at disease onset, however, who will experience a progressive disease course,[11] and DMTs do not prevent neurodegeneration. There is a need therefore for *in vivo* prognostic biomarkers which are sensitive to key neuropathological features of MS, namely demyelination and neurodegeneration, and early longitudinal change.

Conventional MR imaging

Magnetic resonance imaging (MRI) is widely used for diagnosis and tracking MS progression *in vivo* over time but relates poorly to clinical disability – the so-called clinico-radiological paradox.[12] T2 FLAIR hyperintense lesions, which are often perivenular[13-16] and sometimes appear hypointense on T1-weighted images,[17] are relatively non-specific and limit lesion load as an imaging metric. Alongside focal demyelination and brain atrophy, so-called ‘normal-appearing’ white matter (NAWM) may have underlying abnormalities[18] such as decreased fibre density[19] and subtle demyelination,[20] which are not visible on conventional MR images.

Brain atrophy, on the other hand, provides a surrogate measure of neurodegeneration but is a relatively downstream measure. Volumetric measurements may also be confounded by cerebral hydration status and treatment agents for exacerbations of disease.

Quantitative Microstructural MR imaging biomarkers

Microstructural MRI methods, such as magnetisation transfer imaging (MTI) and diffusion-weighted imaging (dMRI), provide potential sources of *in vivo* biomarkers, which are more specific to the pathophysiological characteristics of MS than conventional MRI. MTI signal is indirectly derived from protons 'bound' to macromolecules. 'Bound' protons do not typically contribute to the conventional MRI signal due to T2 much shorter than normal echo times (~10μs) and tend to be myelin-associated in the CNS. The MTI-derived magnetisation transfer ratio (MTR) has been extensively applied in cohorts of RRMS as a measure of myelin integrity.[21] The use of MTR as a surrogate endpoint in large, multi-centre clinical trials is, however, limited by its poor reproducibility and dependence on scanning acquisition parameters.

Biophysical quantitative MTI models more accurately quantify the 'bound' proton pool, but are not practical for large clinical cohorts due to lengthy acquisition times and limited brain coverage. Measures such as magnetisation transfer saturation (MTsat) and inhomogeneous MTR (ihMTR) present clinically feasible alternatives while overcoming some of the limitations of MTR. MTsat accounts for some of the variation in the MTR signal due to T1 relaxation and B1 inhomogeneities,[22] and thus may be more specific to longitudinal changes in myelin integrity.

dMRI, on the other hand, is thought to be sensitive to neuroaxonal structures. dMRI measures depend on the rate of water diffusion, which is altered by the structural architecture of the surrounding environment. In the presence of highly structured white matter tracts, water diffusion is anisotropic; as neuronal degeneration progresses, diffusion is thought to become increasingly isotropic, although glial cell infiltration[23] and crossing fibres may complicate biological interpretation.[24]

Modelling the dMRI signal from multi-shell acquisition protocols, which use several b-values in multiple directions, may help to resolve structural uncertainty. Neurite Orientation Dispersion and Density Imaging (NODDI),[25] for example, compartmentalises the diffusion signal into isotropic (ISOVF) and non-isotropic signal fractions. The non-isotropic signal fraction is further split into restricted (anisotropic) and hindered diffusion signal fractions, plus an orientation dispersion index (ODI).[25] Intraneurite and extraneurite water molecules are thought to be the

source of the restricted diffusion signal (ICVF) and hindered diffusion signal, respectively. ICVF may be a useful marker of neurite (axon and dendrite) density, and is reduced in white matter lesions (WML), although not NAWM, in RRMS compared with healthy control white matter.[26,27] NODDI is nevertheless limited by certain underlying assumptions including the fixed diffusivity rate, and modelling the restricted diffusion compartment as a Watson distribution of impermeable sticks.[25] Since longitudinal studies are currently lacking, the validity of NODDI metrics as neurodegeneration imaging markers of longitudinal change in RRMS remains to be elucidated.[28]

Combining MTI and dMRI markers

Measures which combine MTI and dMRI such as the MR aggregate g-ratio may also better capture the net effects of disease and/or treatment than an individual imaging biomarker alone.[29,30] The g-ratio is a measure of myelin thickness, defined as the ratio of the diameter of the neuronal axon to the diameter of the myelinated axon.[31] Historically a neuropathological measure, an optimal g-ratio of 0.6 for maximum current was theoretically proposed,[31] although later work suggests a higher value (0.72-0.81 in the CNS) is more realistic.[32] Abnormally high g-ratios are indicative of myelin disruption,[33,34] and likely disrupted neuronal conductivity.

Parametric MR aggregate g-ratio maps may be derived by combining MTsat and NODDI data on a voxel-by-voxel basis.[29,30,34-36] Although dependent on a number of prior assumptions, which have been extensively reviewed,[35,37] the MR g-ratio has been validated against *ex vivo* electron microscopy macaque data.[29] In RRMS, elevated g-ratios are associated with an established blood marker of active axonal damage, neurofilament,[30] and the g-ratio structural connectome is disrupted with inter-individual variability related to disease severity.[34] To date, however, g-ratio has not been applied in longitudinal studies of MS.

Rationale and Aims

Given the need for novel *in vivo* biomarkers, which may be candidates for clinical trial surrogate endpoints, the aim of this study was to determine the sensitivity of microstructural MR imaging markers to demyelination and neurodegeneration in patients with RRMS at the point of diagnosis, and their sensitivity to longitudinal change. We hypothesise that MTsat will be more sensitive to early demyelination

than MTR. We further investigate the suitability of microstructural imaging models to RRMS pathology, in comparison to healthy controls, and the potential pitfalls.

Materials and Methods

Participants

Patients with relapsing-remitting multiple sclerosis

Seventy-seven people with recently diagnosed RRMS were recruited to take part in a longitudinal single-centre sub-study of FutureMS at the Anne Rowling Regenerative Neurology Centre (Edinburgh, Scotland). FutureMS[38] is a multicentre, prospective, cross-sectional cohort study of 440 people with RRMS, who were diagnosed within the previous 6 months, according to 2010 McDonald criteria.[39] Individuals with MS were required to be over 18 years of age and the baseline assessment was prior to initiation of any DMT.

The baseline visit (M0) included MRI and clinical assessment, including Expanded Disability Status Scale (EDSS). The follow-up visit (M12) took place one year later with an identical MRI protocol and clinical assessment.

Healthy controls

Twelve healthy volunteers were additionally recruited to receive the same MR imaging protocol as RRMS patient. Exclusion criteria were contraindication to MRI; the protocol was repeated within two weeks to determine test-retest agreement.

Ethical Approval

Approval for the sub-study was obtained from the local Research Ethics Committee (reference REC 15/SS/0233). The study conformed to the Declaration of Helsinki 2000 (amendments in 2002 and 2004) and Good Clinical Practice ICH guidelines. All participants provided written informed consent.

MR image acquisition

All images were acquired on a 3.0 T Siemens Prisma MR system (Erlangen, DE) at the Edinburgh Imaging Facility (Royal Infirmary of Edinburgh) with a 32 channel head coil.

Structural images included a sagittal, 3D T1-weighted MPRAGE; and an axial 2D FLAIR (Supplementary Table 1). MT imaging consisted of three consecutive 3D gradient-echo FLASH sequences (Table 1): two proton density images with and without a Gaussian off-resonance MT saturation pulse (MT_{on} and MT_{off},

respectively), and an additional T1-weighted image. Multi-shell diffusion-weighted 2D echo planar imaging was also performed with 151 diffusion directions and 3 reverse phase encoding volumes (Table 1).

Table 1: Acquisition parameters for magnetisation transfer imaging (MTI) and diffusion-weighted imaging (dMRI).

	Magnetisation Transfer Imaging (MTI)	**Diffusion-weighted imaging (dMRI)**
Sequence	3D FLASH (fast low-angle shot) spoiled gradient echo	2D Echo Planar Imaging (EPI)
Orientation	sagittal	axial
Coil	32 channel	32 channel
FOV (mm)	224 (SI) x 241 (AP)	256 x 256
Acquisition Matrix (mm)	160 x 172	128 x 128
Number of Slices	128	74
Voxel Size (mm)	1.4 (isotropic)	2 (isotropic)
TE (ms)	1.54/4.55/8.49	74
Acceleration factor (in-plane x slice)	2 x 1	2 x 2
TR (ms)	30 (MT_{Off} & MT_{On}) / 15 (MT_{T1w})	4300
Excitation Flip Angle (deg)	5 (MT_{Off} & MT_{On}) / 18 (MT_{T1w})	-
Acquisition Time (m:ss)	6:14 (MT_{Off} & MT_{On} each) / 3:08 (MT_{T1w})	11:12 / 0:35 (rev)
MT Saturation Radiofrequency Pulse	gaussian; 1.2 kHz offset from water frequency; duration 9.984 ms; 500°	-
b-value (s/mm^2) [number of volumes]	-	0 [14], 200 [3], 500 [6], 1000 [64], 2000 [64] & 0 [3] with reverse phase encoding
Number of Diffusion Directions	-	151

MRI Processing

Brain tissue segmentation

Structural MRI data processing is described in detail elsewhere.[38] Briefly, all MR images were first converted from DICOM to NIfTI format (dcm2niix v1.0.20190410[40]). For people with RRMS, WMLs were defined as hyperintensities on T2 FLAIR at M0 and segmented automatically using an in-house thresholding approach,[41] with manual correction where necessary (ITK-SNAP v3.6, http://www.itksnap.org). At follow-up, baseline WML masks were registered to follow-up FLAIR images and manually edited for changes.

Structural T1-weighted MPRAGE images were bias-corrected and brain tissue segmentation was carried out with FreeSurfer (v6.0, https://surfer.nmr.mgh.harvard.edu/) at each time point, followed by FreeSurfer's longitudinal processing stream. Visual quality assurance checks and correction when needed were performed.

MTI parametric maps

Using an in-house MATLAB script (R2018b, software available: https://doi.org/10.7488/ds/2965, requires SPM12 and FSL functions),[42] echoes were summed together to increase the signal-to-noise ratio (SNR)[43] for each MT image (MT_{on}, MT_{off}, and MT_{T1w}). MT_{on} and MT_{T1w} images were registered to the MT_{off} image with a rigid-body transformation (6 degrees of freedom, FSL FLIRT[44,45]). Parametric MTsat and approximation of T1 recovery (T1app) maps were calculated from MT images (MT_{on}, MT_{off}, and MT_{T1w}), as detailed previously.[22,46,47] MTR maps were calculated as MTR = 100 x (MT_{off}-MT_{on}/MT_{off}).

NODDI parametric maps

dMRI processing included brain extraction and removal of bulk motion and eddy-current-induced distortions with FSL (v6.0.1). All dMRI volumes were registered to the first b0 diffusion volume before processing with the NODDI toolbox[25] (v1.0, mig.cs.ucl.ac.uk, MATLAB R2016b) to produce ICVF and ISOVF parametric maps.[38]

G-ratio parametric maps

MTsat maps were registered to dMRI b0 reference volumes before calculating g-ratio maps (FSL epi_reg). Creation of g-ratio maps followed methodology detailed previously,[25,30] using equation:[29]

$$g = \sqrt{\frac{1}{(1 + MVF/AVF)}}$$

MVF is the myelin volume fraction derived from linearly-scaled MTsat maps;[35] AVF is the axonal volume fraction derived from NODDI dMRI data, calibrated in healthy control subjects.[30] The cerebellum was not included in dMRI and g-ratio analyses due to technical inaccuracies.

Mask-to-map registration

For each time-point, tissue segmentations were registered to either the MT_{off} image (FSL FLIRT[44,45]) for MT maps or the first b0 volume of diffusion data for g-ratio maps. To minimise partial volume effects, erosion by one voxel was applied to NAWM masks.

Statistical and Graphical Analyses

All statistical analyses were performed in RStudio (v1.4.1717, R v3.6.1).

Descriptive statistics

Tissue masks were applied to parametric maps (in-house code with *RNifti* package v1.3.0) to output summary statistics (e.g. mean, median).

Relationship between MTR, MTsat and T1app

To compare the distribution of MTR, MTsat and T1app, co-registered indexed voxels for each metric were plotted as two-dimensional histograms (*RNifti* and *ggplot2*::*geom_bin2d* packages in *R*) for healthy control white matter, RRMS NAWM and WML.

Comparison of MTI tissue contrast

NAWM-to-WML tissue contrast and contrast-to-noise were calculated[48] (see Supplementary Methods). Paired t-tests (two-sided, α=0.05/2=0.025) were used to determine whether the difference between MTsat and MTR was significant.

Relationship between NODDI ISOVF, NODDI ICVF and MTsat

The distribution of NODDI parameters and MTsat was compared with two-dimensional histograms of co-registered indexed voxels (*RNifti* and *ggplot2*::*geom_bin2d* packages in *R*) for healthy control white matter, NAWM and WML.

Relationship between g-ratio and underlying metrics

To examine how a longitudinal change in myelin and/or axonal volume fractions would alter the g-ratio, graphical simulations were performed in R (*ggplot* package) using realistic parametric ranges for MTsat and NODDI measures to calculate MVF, AVF and g-ratio. Two-dimensional histograms comparing the distribution of g-ratio against the underlying metrics (NODDI ICVF, NODDI ISOVF and MTsat) were produced (*ggplot2*::*geom_bin2d* package) to determine the dependence of g-ratio on each metric and predict the validity of the g-ratio model for longitudinal change.

Test-retest agreement of microstructural metrics in healthy white matter

Bland-Altman plots[48] were created (*BlandAltmanLeh* R package) to allow assessment of test-retest agreement from healthy control data. Here, the difference in mean values between time points is plotted against the average value over time points for each subject and each microstructural metric. The limits of agreement show the range within which 95% of subjects would be expected to fall if measures were repeated in healthy control white matter, and thus establishes reference levels for pathological change. Sign tests were used to determine whether the difference between time points was significantly different from zero (significance level, $\alpha=0.05$).

Longitudinal change

Longitudinal changes in MTsat, MTR, ISOVF, ICVF and g-ratio across NAWM and WMLs in RRMS patients were first assessed using paired t-tests ($\alpha=0.05$). When significant, follow-up linear mixed modelling (maximum likelihood) was performed to account for potential confounding variables (age, sex, lesion load [as a percentage of intracranial volume] and initiation of DMTs; *R* packages *lme4* and *lmerTest*[49,50]). Whole brain atrophy was also examined with a linear mixed model. Interaction terms were included in models where appropriate. Post-hoc false discovery rate (FDR) correction for multiple comparisons was performed for linear mixed models.

Goodness-of-fit was assessed with Nakagawa's marginal R^2 for mixed models[51] (R package *performance*[52]).

The relationship between longitudinal change across microstructural metrics, and with whole brain atrophy was examined with Pearson's correlation coefficients.

Comparison with healthy control test-retest agreement

To compare longitudinal change over one year with test-retest agreement, the mean difference and limits of agreement from NAWM Bland-Altman plots from test-retest data acquired in healthy controls were superimposed on boxplots of longitudinal change.

Results

Demographics

People with RRMS

77 recruited patients with RRMS underwent imaging at M0. Two were excluded from all analyses as more than six months had passed between diagnosis and imaging. Fourteen datasets were excluded from longitudinal analyses due to poor FreeSurfer tissue segmentation, one subject did not complete the full MRI protocol at follow-up (M12), and dMRI processing failed for two subjects. Longitudinal MTI data were hence available for 62 patients, and dMRI data were available for 60 patients (see Table 2 for demographics).

Healthy Controls

Data from eleven healthy controls (7 females, mean age 44 years [range 27-58 years]) contributed to the final analysis. One healthy control was excluded due to underlying pathology. Due to diffusion processing errors at the second time-point, two controls were excluded from NODDI and g-ratio test-retest analyses.

Table 2: Participant demographics for longitudinal data at M0 (baseline) and follow-up (M12). DMT: disease-modifying therapy; EDSS: Expanded Disability Status Scale score; ICV: intracranial volume; WML: white matter lesions

	Magnetisation transfer imaging		**NODDI ISO/ICVF & g-ratio**	
	M0	**M0 and M12**	**M0**	**M0 and M12**
n (F:M)	75 (59:16)	62 (48:14)	73 (57:16)	60 (46:14)
Mean age [range] in years at M0	37.3 [21.7 to 67.3]	37.6 [21.7 to 67.3]	37.4 [22.3 to 67.3]	37.8 [22.3 to 67.3]
Median EDSS at M0 [range]	2 [0 to 6]	2 [0 to 6]	2 [0 to 6]	2 [0 to 6]
Median EDSS at M12 [range]	-	2.5 [0 to 6.5]	-	2.75 [0 to 6.5]

Number of patients with DMT initiated by M12	-	38 (61.3%)	-	36 (60.0%)
Mean number of days between diagnosis and M0 [range]	69 [7 to 173]	68 [7 to 171]	70 [8 to 173]	69 [8 to 171]
Median disease duration in years [range]	3.4 [0.2 to 33.2] (4 missing)	3.6 [0.2 to 33.2] (2 missing)	3.4 [0.2 to 33.2] (2 missing)	3.55 [0.2 to 33.2] (2 missing)
Mean change in WML volume over 1 year (as % of ICV, abs. diff) [range]	-	0.235% [0.028% to 0.592%]	-	0.236% [0.028% to 0.592%]

Relationship between MTR, MTsat and T1app

Healthy control white matter

In healthy controls, MTsat parametric maps show visibly better white-to-grey matter contrast than MTR maps (Figure 1). Two-dimensional density plots show a strong negative linear association between MTsat and T1app within myelin-dense areas (i.e. high MTsat, Supplementary Figure 1A), which fades into an exponential decay at low MTsat values. Conversely, there appears to be a weak positive linear relationship between MTR and T1app in myelin-dense tissue (MTR < 40%, T1app > 2s), although the overall trend is one of a broad negative relationship (Supplementary Figure 1B). The relationship between MTR and MTsat appears to follow a hyperbolic tangent, with a plateau in areas of high myelin density (Supplementary Figure 1C).

Figure 1: Example magnetisation transfer ratio (MTR, top row), magnetisation transfer saturation (MTsat, middle row) and approximation of T1 recovery (T1app, bottom row) parametric maps for a healthy control subject.

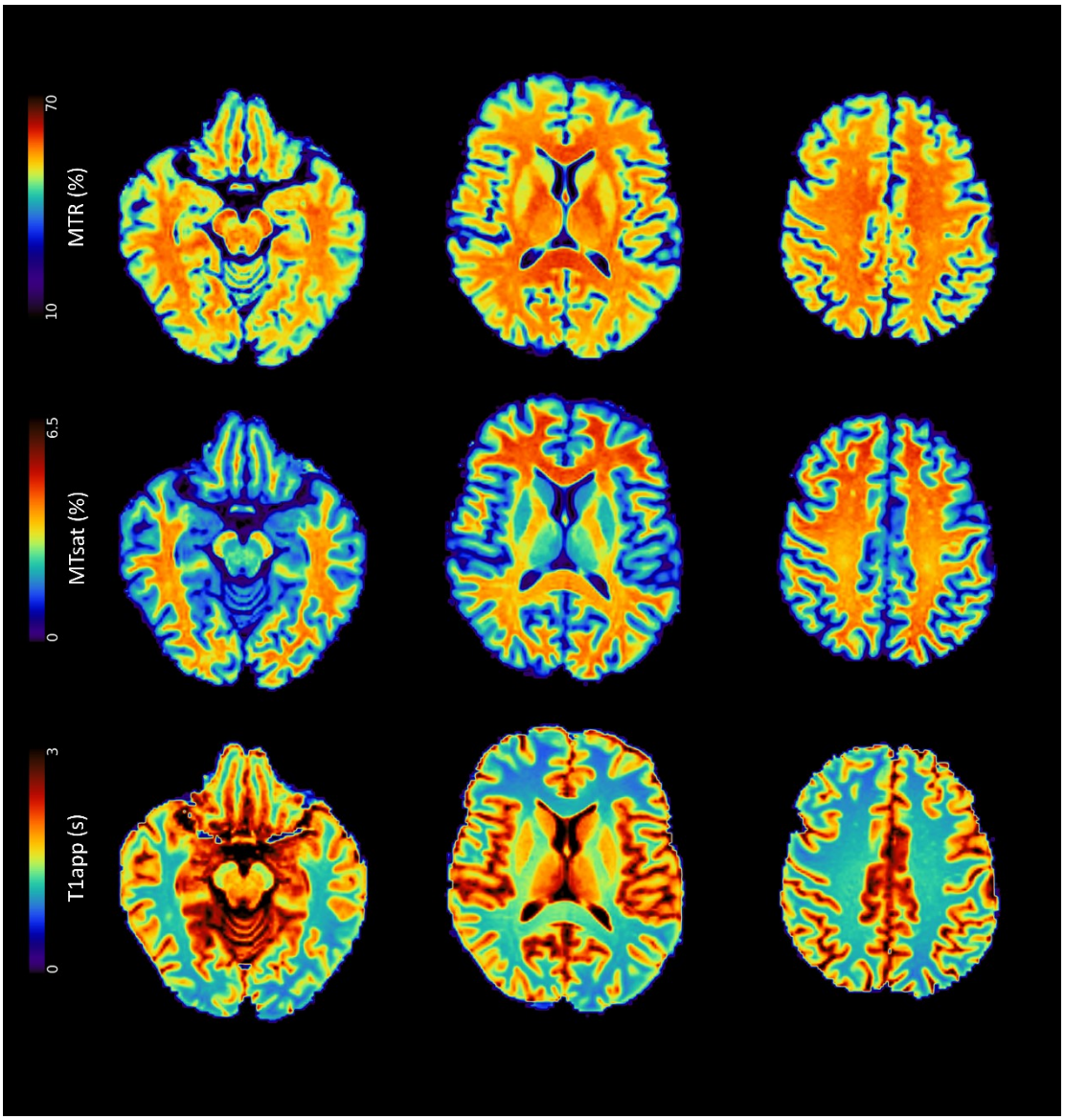

'Normal-appearing' white matter

In RRMS NAWM, two-dimensional density plots show broadly similar relationships between MT parameters on a voxel-by-voxel basis as control white matter (Figure 2). There is a greater spread of MTsat and MTR values, however, at the lower end. The distribution of NAWM T1app does not appear to differ from healthy control white matter (Supplementary Figure 1).

Figure 2: Two dimensional density plots show the relationship between T1app and (A) MTsat, and (B) MTR, and between (C) MTR and MTsat in normal-appearing white matter in recently diagnosed relapsing-remitting multiple sclerosis at baseline (n=75).

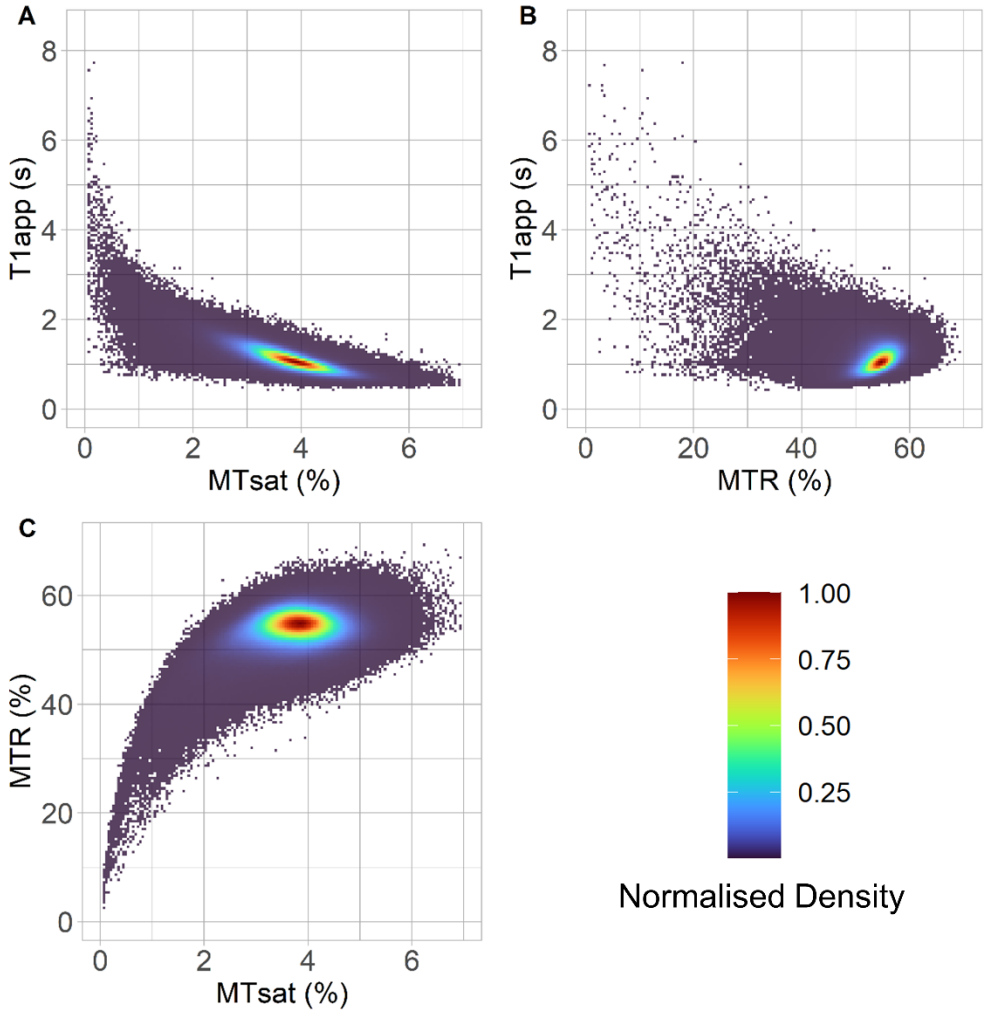

White matter lesions

White matter pathology was more visible on MTsat maps compared with MTR for patients with RRMS (Figure 3). Paired t-tests confirmed that MTsat had significantly higher NAWM-to-WML contrast (mean diff.: 16.9 [95%CI 15.96 to 17.89], t(74)=34.97, p<0.001) and CNR (mean diff.: 0.51 [95% CI 0.47 to 0.55], t(74)=26.7, p<0.001) than MTR (Supplementary Table 2).

Figure 3: Example magnetisation transfer ratio (MTR, top row), magnetisation transfer saturation (MTsat), and T1app (bottom row) parametric maps for a person with recently diagnosed relapsing-remitting multiple sclerosis.

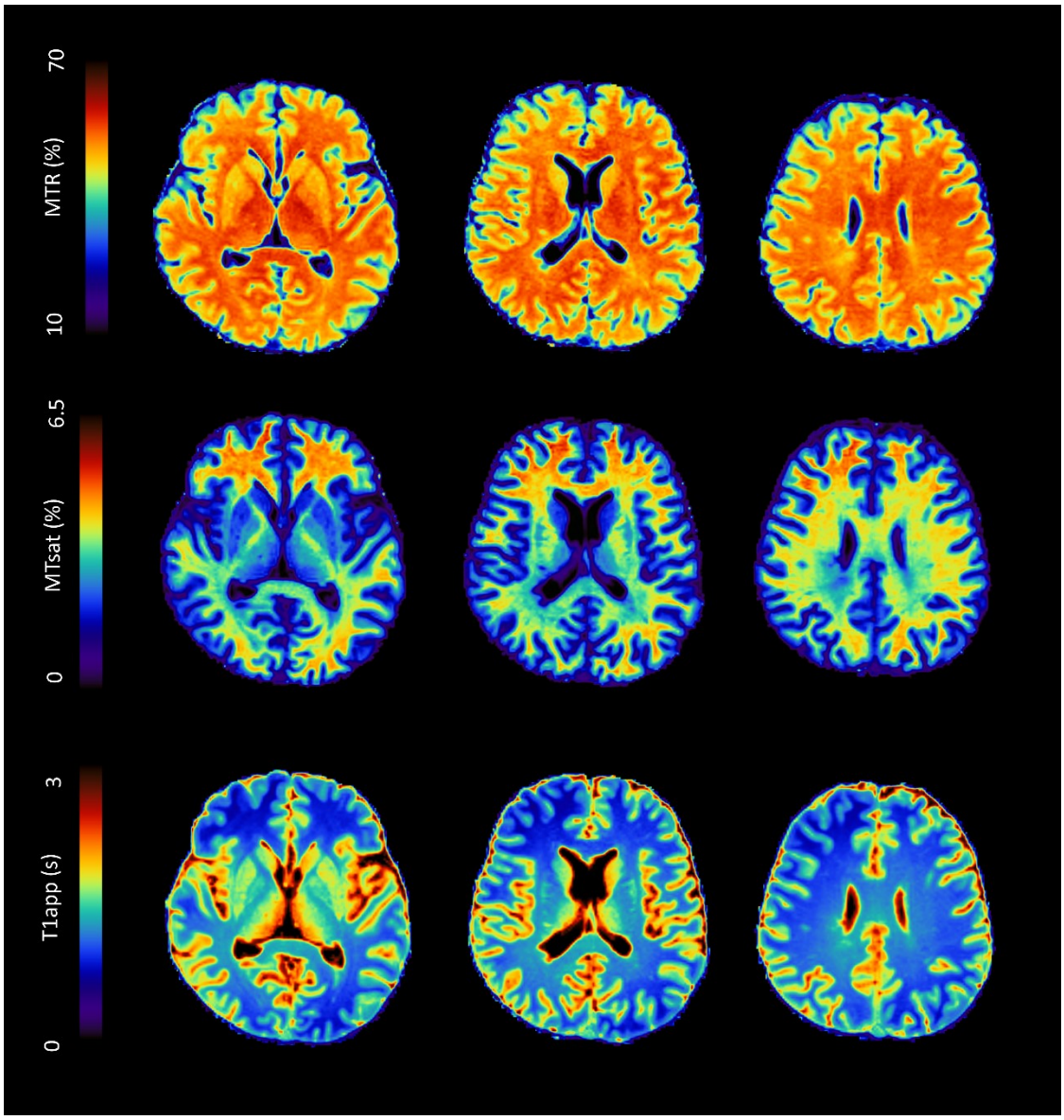

There was a wide range of MTsat values in lesions across the cohort (Figure 4). The distribution of MTsat values was lower in WML compared with NAWM (Figure 2) and control white matter (Supplementary Figure 1), and higher for T1app. MTR and MTsat were also positively related (Figure 4C).

Figure 4: Two dimensional density plots show the relationship between T1app and (A) MTsat, and (B) MTR, and between (C) MTR and MTsat in white matter lesions in recently diagnosed relapsing-remitting multiple sclerosis at baseline (n=75).

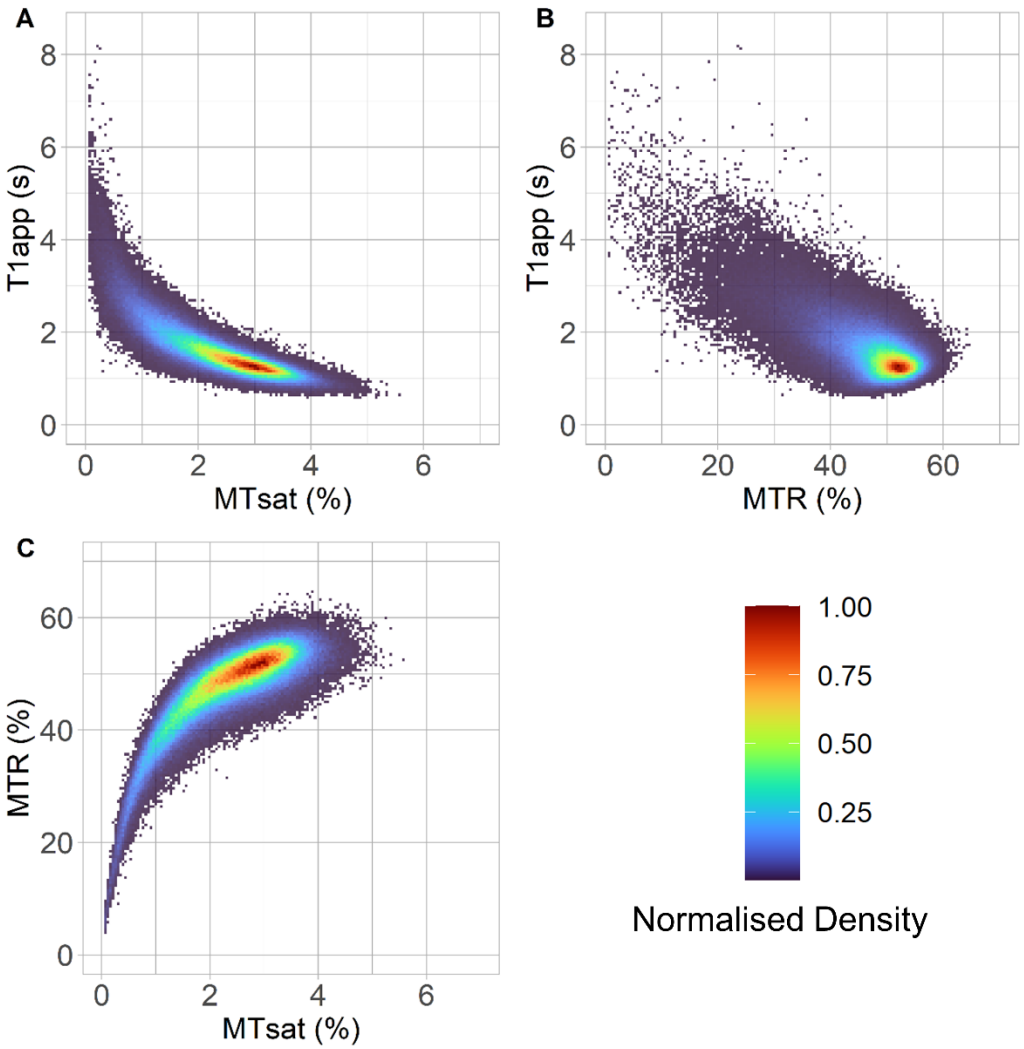

Relationship between NODDI ISOVF, NODDI ICVF and MTsat

Healthy control white matter

In healthy controls, there is no clear relationship between MTsat and NODDI metrics (Supplementary Figure 2A-B). There is a weak positive relationship between NODDI ICVF and NODDI ISOVF (Supplementary Figure 2C), although NODDI ISOVF remain low across healthy white matter (Figure 5).

Figure 5: Example white matter NODDI parametric maps for a healthy control subject: intracellular (restricted) volume fraction (top row) and isotropic volume

fraction (bottom row). Parametric maps are overlaid on the first b0 diffusion-weighted volume. Colour scale ranges are adjusted for optimal visibility for each metric.

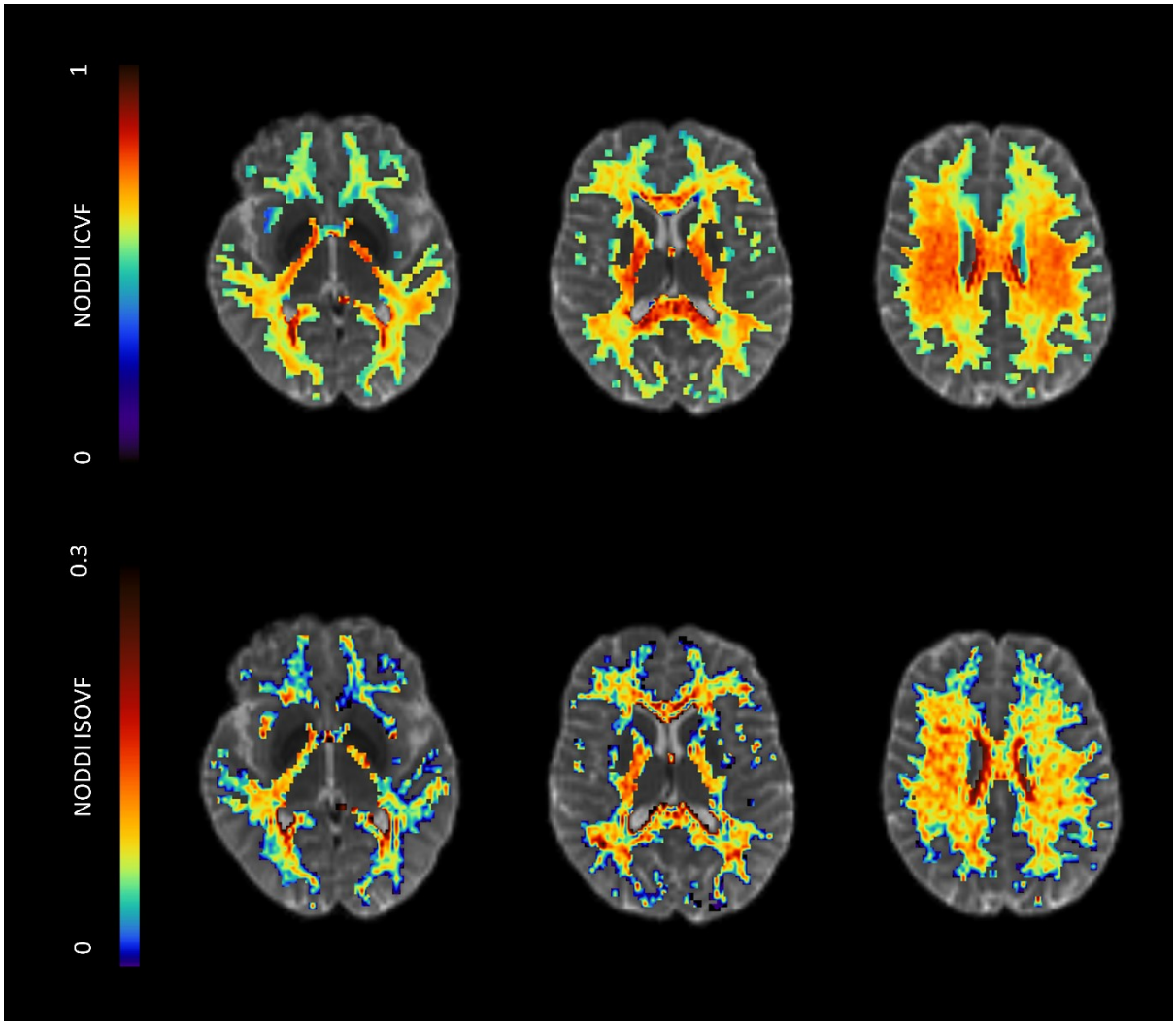

'Normal-appearing' white matter

Similarly to healthy white matter, in NAWM, there is no clear relationship between NODDI measures and MTsat (Figure 6A-B). Overall, NODDI ISOVF is slightly higher in NAWM than healthy white matter, while NODDI ICVF is lower (Figure 6B-C and Supplementary Figure 2B-C for control white matter).

Figure 6: Two dimensional density plots show the relationship between (A) NODDI ICVF and MTsat, (B) NODDI ISOVF and MTsat, and (C) NODDI ICVF and NODDI ISOVF, and between g-ratio and (D) NODDI ISOVF, (E) NODDI ICVF and (F) MTsat in cerebral normal-appearing white matter at baseline in people recently diagnosed with relapsing-remitting multiple sclerosis (n=73).

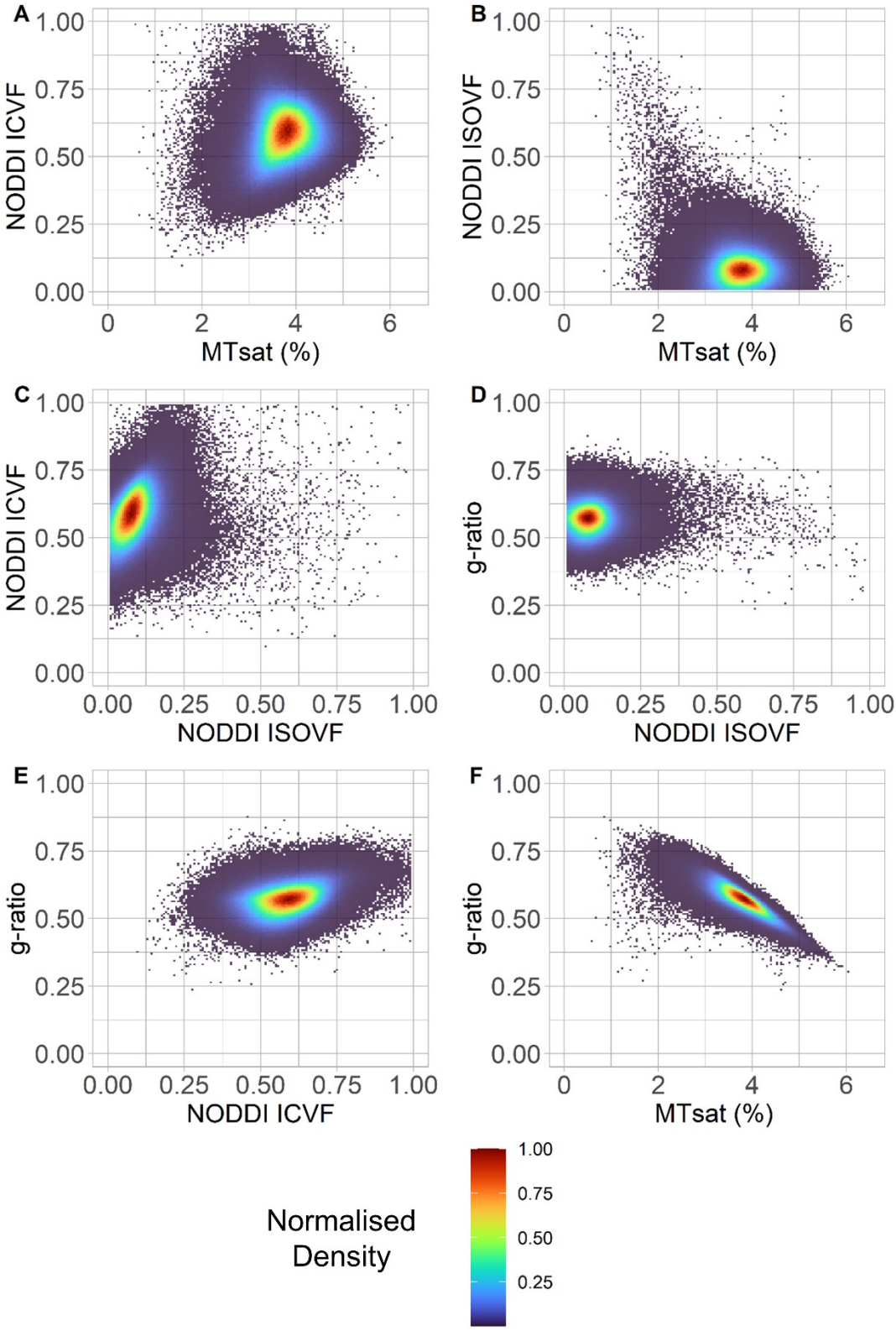

White matter lesions

In WML, NODDI ICVF was visibly lower than in NAWM (Figure 7). There was a broadly linear positive association between NODDI ICVF and MTsat (Figure 8A). NODDI ISOVF, however, is non-linearly related to MTsat; ISOVF values above ~0.25 are only seen at lower MTsat values (around <2%, Figure 8B). Conversely, the weak positive relationship between NODDI ICVF and ISOVF observed in NAWM appears to breakdown in lesions.

Figure 7: Example intracellular volume fraction (ICVF, top row) and isotropic volume fraction (ISOVF, bottom row) NODDI parametric maps for a person with recently diagnosed relapsing-remitting multiple sclerosis. Arrows: white matter lesion.

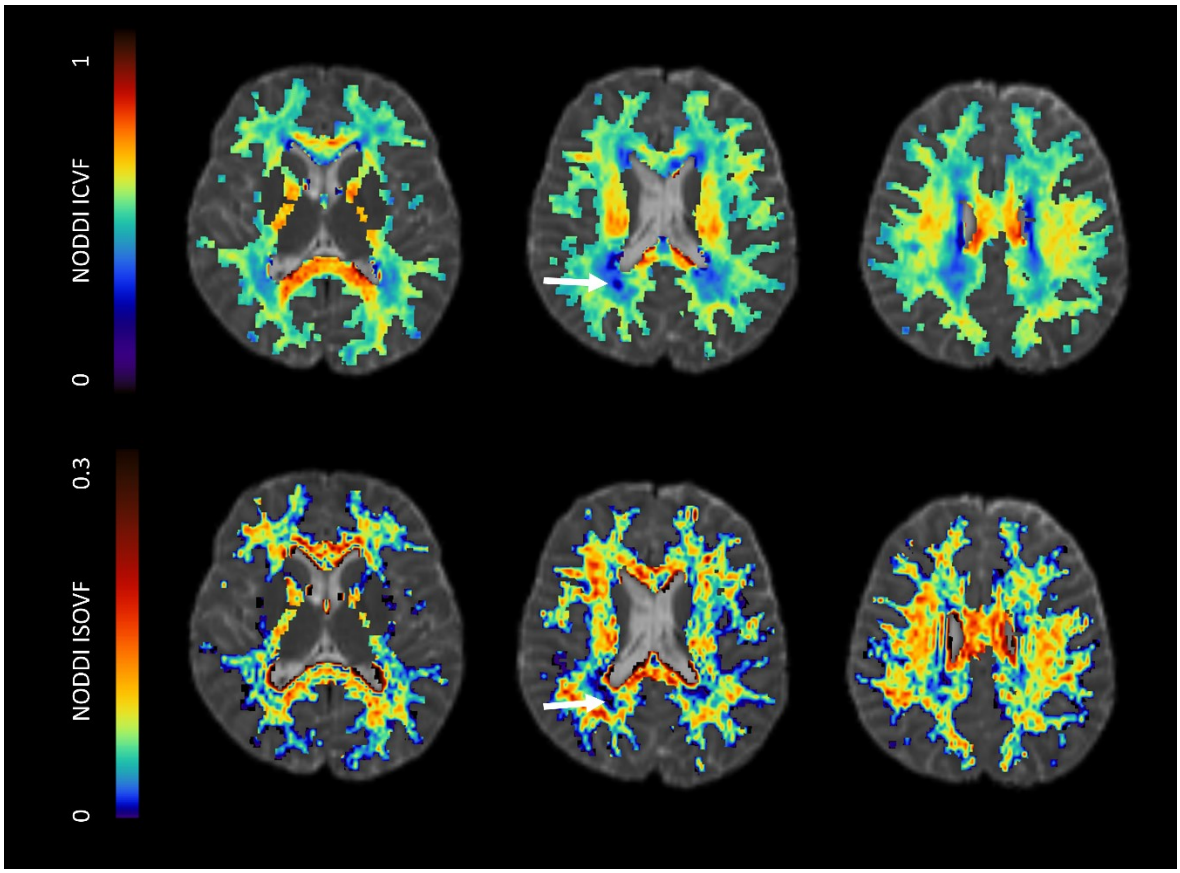

Figure 8: Two dimensional density plots show the relationship between (A) NODDI ICVF and MTsat, (B) NODDI ISOVF and MTsat, and (C) NODDI ICVF and NODDI ISOVF, and between g-ratio and (D) NODDI ISOVF, (E) NODDI ICVF and (F) MTsat in white matter lesions, at baseline in people recently diagnosed with relapsing-remitting multiple sclerosis (n=73).

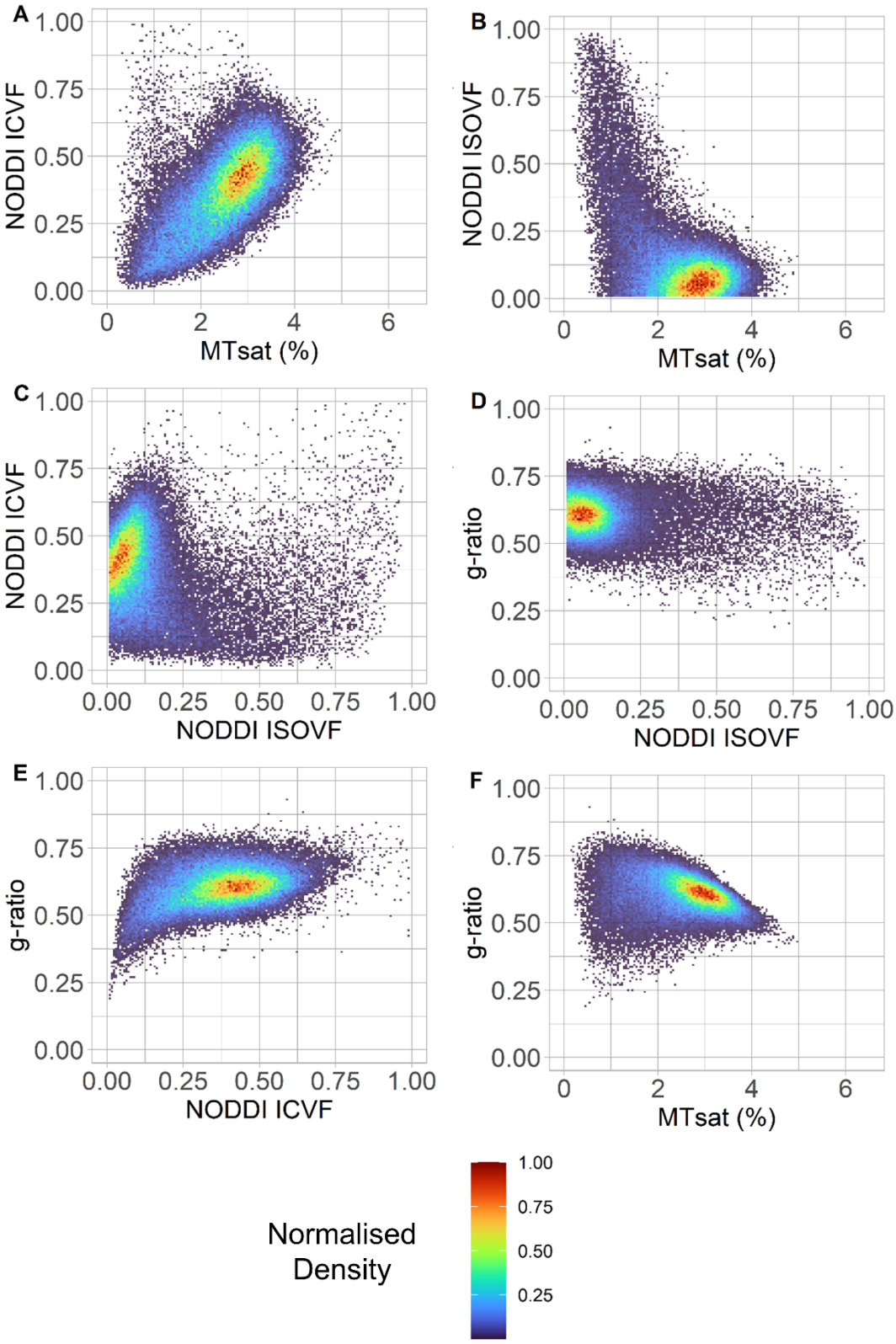

Relationship between g-ratio and underlying metrics

Simulations

Simulations (Supplementary Figure 3) show the competing effects of changes in MTsat and NODDI metrics on g-ratio. As MTsat decreases, the g-ratio increases, when NODDI metrics are held constant. An increase in ICVF, however, may also increase the g-ratio. An increase in ISOVF, on the other hand, results in a decrease in g-ratio.

Figure 9: Example white matter parametric maps for a healthy control subject: myelin volume fraction (top row), axonal volume fraction (middle row), and g-ratio (bottom row). Parametric maps are overlaid on the first b0 diffusion-weighted volume. Colour scale ranges are adjusted for optimal visibility for each metric.

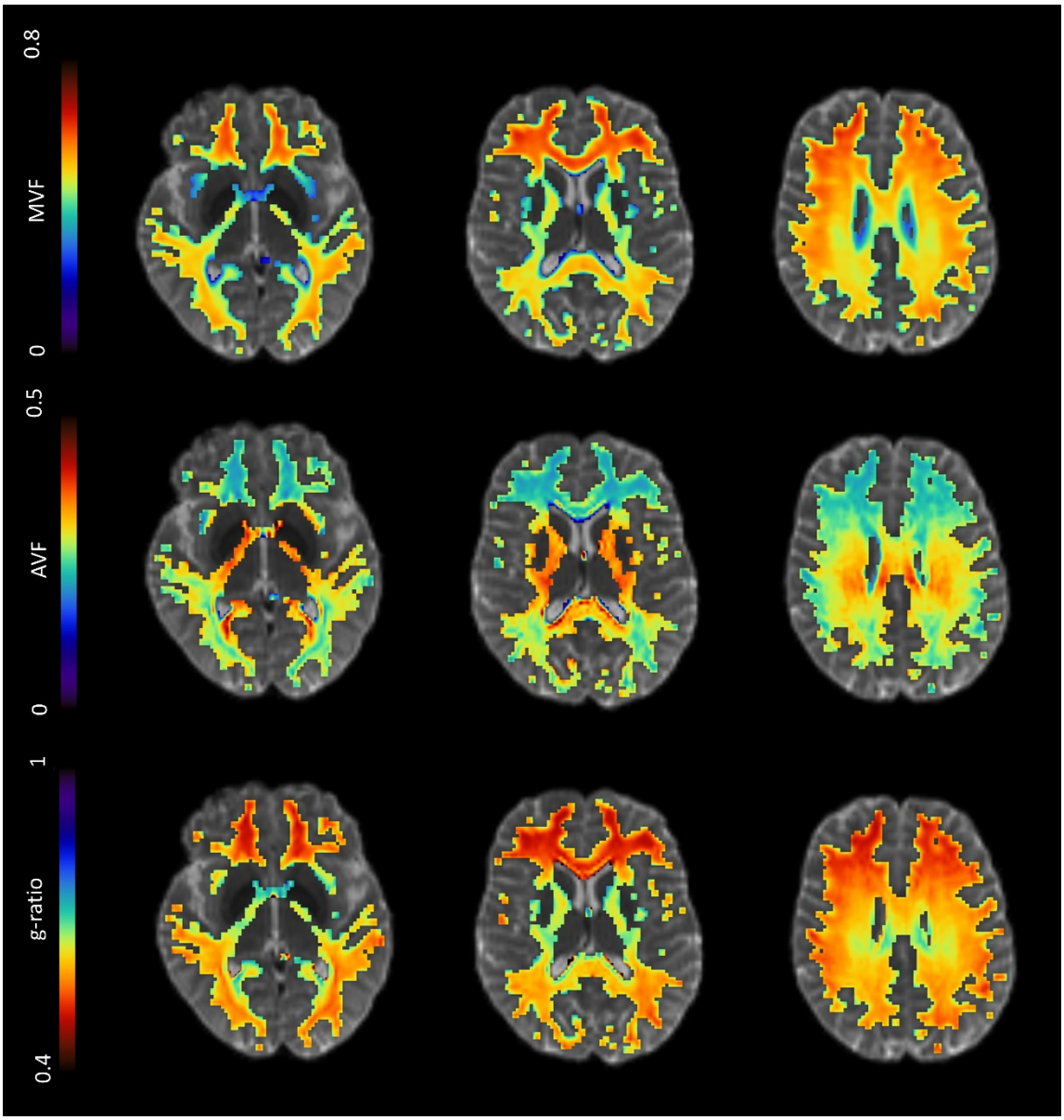

Healthy white matter

In white matter, g-ratio is largely linearly dependent on MTsat (Supplementary Figure 2F and Figure 9), although as ICVF increases, g-ratio tends to increase (Supplementary Figure 2E). There is no apparent relationship between NODDI ISOVF and g-ratio at the values seen in healthy white matter (Supplementary Figure 2D).

Figure 10: Example myelin volume fraction (MVF, top row), axonal volume fraction (AVF) and g-ratio parametric maps for a patient with recently diagnosed relapsing-remitting multiple sclerosis.

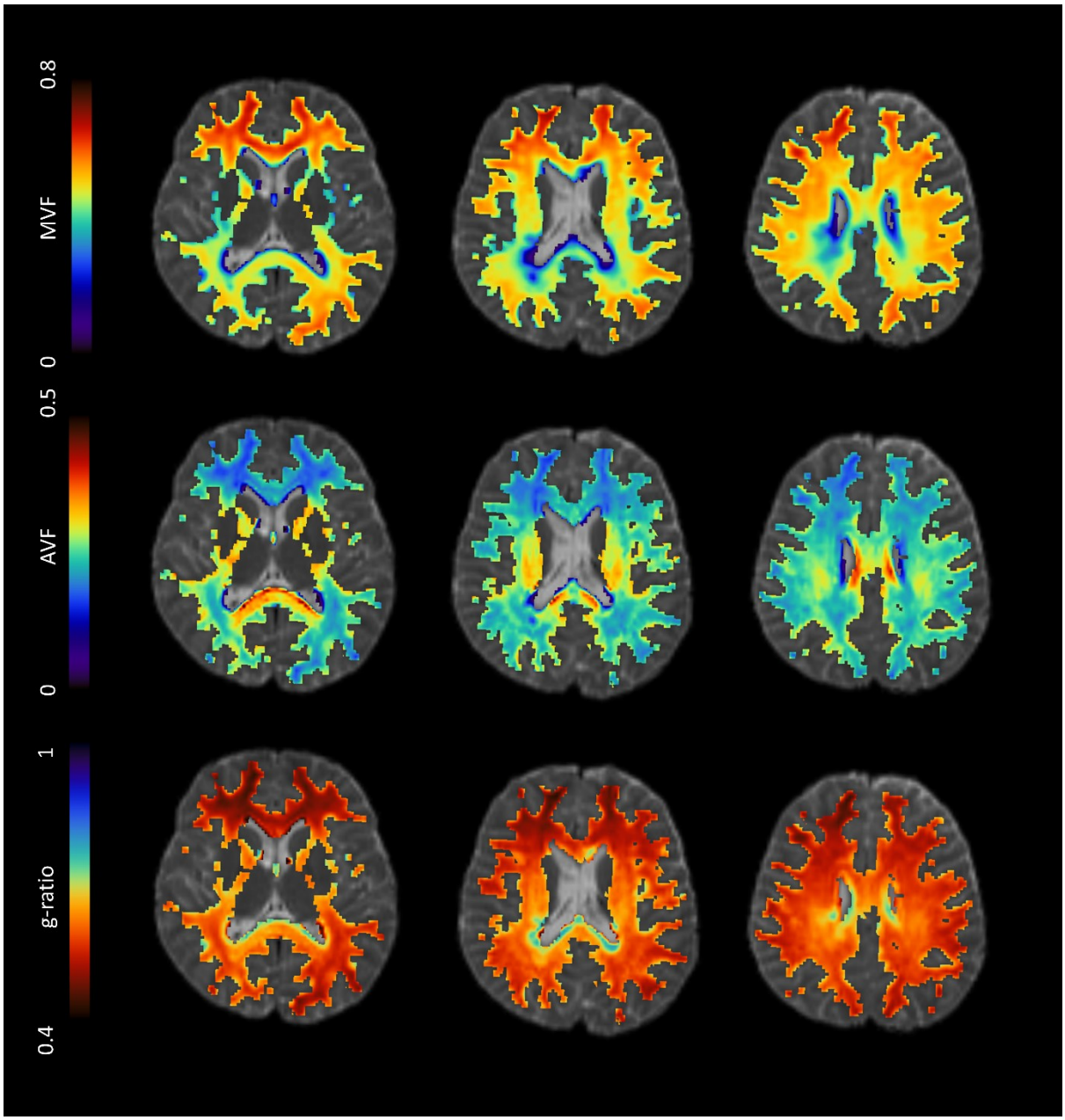

'Normal-appearing' white matter

In people with RRMS, g-ratio (Figure 10) at M0 was similarly highly dependent on MTsat in NAWM, with no clear relationship with NODDI ISOVF and a weak positive dependence on NODDI ICVF (Figure 6D-F).

White matter lesions

In WML, the dependence of g-ratio on MTsat was weaker than in NAWM, particularly at low MTsat values (<2%, Figure 8F) where greater variability in g-ratio was observed. Similarly, the relationship between NODDI ICVF and g-ratio was also generally weaker than in NAWM, with the exception of low NODDI ICVF (<0.25, Figure 8E) where a sharp decrease in g-ratio values was seen. High NODDI ISOVF values, however, appear to negatively influence g-ratio values, although the effect is small (Figure 8D)

Test-retest agreement

In healthy white matter, sign test and Bland-Altman plots (Supplementary Figures 4-5) show that the mean difference in MTI, NODDI and g-ratio did not differ from zero between time points (all p>0.05, Table 3). Descriptive statistics and Bland-Altman limits of agreement for all metrics are reported in Table 3.

*Table 3: Mean (standard deviation) MTI, NODDI and g-ratio values in healthy control white matter (n=11, except where indicated *n=9). P-values are given for two-sided sign tests for matched pairs.*

	Time point 1	Time point 2	Mean difference	p-value (uncorrected)	Bland-Altman Limits of Agreement
MTsat (%)	3.74 (0.13)	3.78 (0.11)	0.04 (0.09)	0.549	±0.186
MTR (%)	54.51 (0.66)	54.25 (0.70)	-0.26 (0.68)	1.00	±1.341
T1app (s)	1.129 (0.07)	1.101 (0.05)	-0.028 (0.06)	1.00	±0.118
NODDI ISOVF	0.086 (0.008)	0.086 (0.008)*	-0.001 (0.003)*	1.00	±0.0057*

NODDI ICVF	0.610 (0.022)	0.609 (0.020)*	-0.002 (0.003)*	0.180	±0.0064*
g-ratio	0.587 (0.015)	0.581 (0.012)*	-0.005 (0.011)*	0.508	±0.024*

Longitudinal change in 'normal-appearing' white matter

In NAWM, paired t-tests showed a significant decrease in MTsat and significant increases in NODDI ICVF and g-ratio (Table 4). Group mean changes over time (Table 4) were lower than the limits of agreement established from healthy control data (Table 3), although a small number of subjects exceeded these limits (Supplementary Figure 6). MTR and NODDI ISOVF did not change significantly over one year.

*Table 4: Descriptive statistics and paired t-tests for MTI (n=62), g-ratio and NODDI (n=60) data in 'normal-appearing' white matter. MTsat: magnetisation transfer saturation; MTR: magnetisation transfer ratio; ICVF: intracellular volume fraction; ISOVF: isotropic volume fraction; SD: standard deviation; M0: baseline; M12: one year follow-up. *excludes cerebellum for g-ratio and NODDI metrics*

	'Normal-appearing' white matter*				
	M0	**M12**	**mean diff. (SD)**	**paired t-test**	
				t-value	**p-value (uncorrected)**
MTsat (%)	3.80 [3.43 to 4.07]	3.77 [3.39 to 4.25]	-0.03 [0.12]	-2.19	0.033
MTR (%)	54.25 [50.80 to 56.28]	54.24 [52.02 to 56.39]	-0.01 [0.82]	-0.079	0.94
g-ratio	0.57 [0.538 to 0.609]	0.574 [0.523 to 0.625]	0.004 [0.012]	2.60	0.012

NODDI ISOVF	0.075 [0.054 to 0.097]	0.074 [0.044 to 0.096]	0 [0.007]	-0.43	0.67
NODDI ICVF	0.577 [0.504 to 0.640]	0.579 [0.499 to 0.639]	0.002 [0.007]	2.29	0.025

After controlling for age, lesion load, sex, initiation of DMTs and interaction terms, linear mixed models showed that the effect of time on NAWM g-ratio (β = 0.005, t(75.91) = 3.08, p = 0.003, Supplementary Table 3) and NAWM NODDI ICVF (β = 0.003, t(90.89) = 3.51, p = 0.001, Supplementary Table 4) remained significant and survived correction for multiple comparisons. The effect of time on NAWM MTsat was also significant (β = -0.040, t(79.26) = -2.60, p = 0.011, Supplementary Table 5) but not after correction for multiple comparisons.

In NAWM, one year change in g-ratio was strongly associated with change in MTsat (Pearson's R^2 = 0.98, Supplementary Figure 7). Correlations between change in NODDI metrics and g-ratio were weak (Pearson's R^2 = 0.18 and 0.11 for NODDI ICVF and ISOVF, respectively), as were associations between longitudinal change in MTsat and NODDI metrics (Pearson's R^2 = 0.11 for both ICVF and ISOVF).

Longitudinal change in white matter lesions

In WMLs, paired t-tests revealed significant longitudinal increases in MTsat, MTR, NODDI ISOVF and NODDI ICVF (Table 5). Group mean changes in MTsat and MTR were lower than limits of agreement established in healthy control white matter (Table 3) whereas the mean increases in NODDI ISOVF and ICVF were greater than the limits of agreement. A large number of individual subjects exceeded both positive and negative limits of agreement for NODDI ISOVF and NODDI (Supplementary Figure 6). There was no change in g-ratio within WMLs over the same time period.

Linear mixed models showed that the increase in NODDI ICVF (β = 0.017, t(80.64) = 6.95, p < 0.001, Supplementary Table 6), MTsat (β = 0.059, t(82.58) = 3.65, p < 0.001, Supplementary Table 7), and NODDI ISOVF (β = 0.011, t(74.85) = 5.56, p < 0.001, Supplementary Table 8) over one year remained significant after correction for confounding variables and interaction terms. All three effects survived correction

for multiple comparisons. The change in MTR over time, however, was not significant (β = 0.24, t(79.48) = 1.60, p = 0.113, Supplementary Table 9).

In WMLs, the association between longitudinal change in g-ratio and other metrics was weak (Pearson's R^2 = 0.16, 0.17 and 0.11 for MTsat, NODDI ICVF and ISOVF, respectively, Supplementary Figure 8). Change in MTsat within WMLs was moderately associated with NODDI ICVF (Pearson's R^2 = 0.29) and weakly negatively associated with NODDI ISOVF (Pearson's R^2 = 0.16).

*Table 5: Descriptive statistics and paired t-tests for MTI (n=62), g-ratio and NODDI (n=60) data in T2 FLAIR white matter lesions. MTsat: magnetisation transfer saturation; MTR: magnetisation transfer ratio; ICVF: intracellular volume fraction; ISOVF: isotropic volume fraction; SD: standard deviation; M0: baseline; M12: one year follow-up. *excludes cerebellum for g-ratio and NODDI metrics*

	White matter lesions*				
	M0	**M12**	**mean diff. [SD]**	**paired t-test**	
				t-value	**p-value (uncorrected)**
MTsat (%)	2.35 [1.74 to 3.02]	2.43 [1.80 to 3.06]	0.08 [0.1]	6.34	<0.001
MTR (%)	47.33 [43.39 to 52.58]	47.8 [43.45 to 51.73]	0.47 [1.05]	3.52	<0.002
g-ratio	0.61 [0.541 to 0.683]	0.61 [0.546 to 0.683]	0 [0.011]	0.06	0.950
NODDI ISOVF	0.095 [0.036 to 0.182]	0.105 [0.051 to 0.188]	0.010 [0.017]	4.54	<0.001
NODDI ICVF	0.379 [0.273 to 0.458]	0.400 [0.297 to 0.479]	0.021 [0.02]	8.30	<0.001

Lack of relationship with whole brain atrophy

After adjusting for covariates, there was no signifcant decrease in whole brain volume over one year (Supplementary Table 10) and there was no relationship between whole brain atrophy and any of the microstructural measures that showed significant change over time (Supplementary Figure 9).

*Table 6: Summary of linear mixed model results. MTsat: magnetisation transfer saturation; MTR: magnetisation transfer ratio; NODDI: neurite orientation dispersion and density index; ISOVF: isotropic volume fraction; ICVF: intraneurite volume fraction; NAWM: normal-appearing white matter; WML: white matter lesions; * significant after FDR correction for multiple comparisons*

	Longitudinal Change	
	NAWM	WML
MTsat	↓	↑ *
MTR	-	-
	cerebral NAWM	cerebral WML
g-ratio	↑ *	-
NODDI ISOVF	-	↑ *
NODDI ICVF	↑ *	↑ *

Discussion

Summary of Results

In this study, we examine the sensitivity of microstructural MR imaging measures to demyelination and neurodegeneration in RRMS at diagnosis. We show that MTsat maps have better NAWM-to-WML contrast than MTR, and we demonstrate a relatively linear negative relationship between T1app and MTsat, compared with a complex relationship between MTR and T1app, in myelin-dense tissue. We additionally illustrate that, in WMLs in which MT values are low, MTsat is non-linearly dependent on T1app, while MTR is broadly linearly dependent on T1app.

We further explore the relationship between dMRI-derived NODDI measures and MTsat. In healthy control white matter and NAWM, we find little relationship between NODDI measures and MTsat although unexpectedly, we observe a weak positive relationship between NODDI ICVF and ISOVF. In WML, however, this relationship breaks down at higher ISOVF values. Moreover, in contrast to NAWM, we see a broad positive linear relationship between NODDI ICVF and MTsat in WML, and high NODDI ISOVF only where MTsat is lower than NAWM values.

We then simulate how combining MTsat and NODDI measures as an aggregate MR g-ratio may aid or impede the longitudinal measurement of demyelination and neurodegeneration. We show that the g-ratio is inversely related to MTsat and thus myelin integrity, but that a positive dependence on NODDI ICVF and a negative dependence on NODDI ISOVF remain, complicating biological interpretation of longitudinal change. Using healthy control white matter and patient NAWM data, we nevertheless show that the contribution of NODDI ISOVF and, to a lesser extent, ICVF to variance in g-ratio is small compared to MTsat. Conversely, in WML, low MTsat and/or NODDI ICVF values may erroneously lower g-ratio estimates.

With these observations in mind, we apply microstructural metrics, including g-ratio, to longitudinal data acquired at baseline and one year follow-up from patients with early RRMS. In NAWM, we find a longitudinal increase in g-ratio and NODDI ICVF and, to a lesser extent, a decrease in MTsat (see Summary Table 6). In WMLs, we see an increase in MTsat, NODDI ICVF and NODDI ISOVF over one year. No change in MTR, NODDI ISOVF in NAWM, or WML g-ratio was observed.

Finally, we compare longitudinal patient data with healthy control test-retest data to determine whether effect sizes are likely to be due to real pathological change. We find that, despite significant groupwise changes, the majority of individual patients remain within established limits of agreement in healthy white matter, with the exception of NODDI measures in cerebral WML.

MT metrics and T1 relaxation effects

MTI is highly sensitive to protons 'bound' to macromolecules, which are abundant in myelin in the brain. The 'bound' pool is substantially reduced in WML compared with NAWM, resulting in lower MTsat/MTR values which are likely attributable to demyelination.[53] Our results, illustrating that MTsat has improved contrast and CNR compared with MTR, are in line with previous work showing higher intra-thalamic contrast for MTsat than MTR[54] and visibly high NAWM-to-WML contrast on MTsat maps.[22,55]

The improved NAWM-to-WML contrast for MTsat compared with MTR may be due to the disentanglement of T1 recovery from MT in myelin-dense areas and inherent correction for B1 inhomogeneities.[22] MTR is dependent on a complex relationship between T1 recovery, TR and flip angle, the latter of which may vary with across the brain with spatial inhomogeneities.[56] MTsat, however, is relatively independent of these influences. In practice, our results show that, whereas T1 alters MTR in an unpredictable fashion in NAWM, T1 prolongation consistently coincides with a decrease in MTsat. Moreover, the additional inherent correction for B1 inhomogeneities in the MTsat measures may further reduce noise compared with MTR. MTsat may therefore permit earlier detection of subtle demyelination in NAWM than MTR.

In areas of low myelin content, however, results in our study demonstrate that MTsat closely resembles T1 recovery. This may indicate that a 'floor effect' exists for MTsat beyond which MTsat may provide equivalent information to a quantitative T1 measure with B1 correction. Such an approach may be applied in areas with severe tissue destruction such as 'black hole' lesions, which are defined by sufficiently prolonged T1 to be obvious by visual inspection on T1-weighted sequences.[57,58]

Myelin-sensitive imaging versus diffusion-weighted imaging

As elaborated previously, accurate derivation of the MR g-ratio requires accurate estimation of MVF and AVF.[35,37] In our study, the lack of relationship between MTsat and NODDI measures in NAWM supports the assumption that dMRI is relatively insensitive to myelin and, conversely, that MTI is insensitive to axonal structure and free water content; that is they are independent measures. Our finding reinforces the idea that combining microstructural techniques, which are specific to different aspects of neuronal architecture, may aid accurate modelling of tissue microstructure.

On the other hand, we see a positive association between MTsat and NODDI ICVF in WML in patients with recently diagnosed RRMS. Since MTsat serves as a proxy for myelin[53] and ICVF for axonal density,[59] this finding is consistent with the presence of both demyelination and axonal degeneration in early RRMS. This additionally accords with previous findings of a proportional relationship between myelin water fraction (MWF) and NODDI ICVF in lesions in a mixed MS cohort.[27]

The skewed distribution of NODDI ISOVF in WMLs, however, strongly suggests a 'floor' threshold effect for MTsat at ~2%. Below this threshold, high ISOVF values dominate, and are indicative of a large free water component and severe tissue destruction. Moreover, this threshold approximately corresponds to the threshold below which MTsat resembles T1 recovery. MTsat, therefore, may not offer additional value as a marker of MS pathology in severely damaged WML.

Somewhat surprisingly, given a weak negative association reported elsewhere,[60] NODDI ICVF and ISOVF were weakly positively related at low ISOVF values. A larger 'hindered' diffusion volume fraction (ECVF), assumed to be due to glial cells infiltration and cell bodies, could lead to both a reduction in ISOVF and ICVF. In healthy subjects, larger ISOVF has been reported elsewhere in highly structured white matter (e.g. splenium of corpus callosum) compared with, for example, the putamen and thalamus.[61] This was previously attributed to greater perpendicular diffusion in large axons but could also be explained by partial volume effects at CSF borders, such as between the corpus callosum and ventricles. Alternatively, ISOVF and ICVF measures may be similarly affected by noise. ISOVF, in particular, is

known to be susceptible to noise[62] and confounded by T2 relaxation;[63] moreover, the fixed intrinsic diffusivity assumption may simply not hold true.

Simulating the MR g-ratio and potential pitfalls

Simulating the impact of concurrent changes in microstructural metrics on the g-ratio sheds light on the complexity of interpreting longitudinal change in MR imaging markers. As expected with demyelination in RRMS, decreasing MTsat leads to an increase in the MR g-ratio, and supports the use of g-ratio as means to link neuronal conductivity to longitudinal changes in white matter integrity in RRMS.

Significant changes in NODDI measures, however, are problematic for the interpretation of the g-ratio. In RRMS, axonal density, measured here with NODDI ICVF, is expected to decrease with neurodegenerative processes and free water (i.e. ISOVF) is expected to increase as tissue destruction becomes more pronounced. Simulations suggest, however, that a large increase in ISOVF would lead to a decrease in g-ratio while conversely a large decrease in ICVF, without a concomitant increase in MTsat, could lead to a decrease in g-ratio. While the latter scenario is expected to be unlikely in MS pathology, increases in ISOVF may be more common, particularly in WML; thus rendering the g-ratio model flawed in severely damaged WML and as a longitudinal imaging marker. Nonetheless, the g-ratio remains of use in NAWM, where large changes in ISOVF and ICVF are not expected. Although the g-ratio is clearly attractive as a parameter with a specific histopathological correlate, our data suggest that it may not provide significant additional information to MTsat.

Longitudinal changes in microstructural imaging metrics

Normal-appearing white matter

The longitudinal decline in MTsat in NAWM suggests that subtle loss of myelin integrity occurs in recently diagnosed RRMS, which cannot be seen on conventional T2-weighted FLAIR. Longitudinal MTsat data in RRMS have not previously been reported, although MTsat has been shown to be lower in NAWM in MS than healthy control white matter.[64] The reduction in MTsat in NAWM over one year in our study was small in comparison to variance in test-retest healthy control white matter, however, and the effect did not survive correction for multiple comparisons. This suggests that, although there may be a weak group-wise longitudinal change in

MTsat, measurement error may limit the application of measuring longitudinal change in NAWM MTsat on an individual patient level (e.g. for clinical decision-making). Furthermore, patients in our study were recruited shortly after diagnosis, and the resolving effects associated with the acute inflammatory episode that prompted diagnosis at baseline are potential confounds. Heterogeneous demyelination and myelin repair across NAWM could therefore also explain the weak effect over a relatively short period of time.

Nevertheless, the lack of change in NAWM MTR suggests that MTsat is more sensitive to early RRMS pathology. MTsat and MTR are both sensitive to protons 'bound' to macromolecules within the lipid bilayers of myelin; the sensitivity of MTR to T1 recovery effects and B1 inhomogeneities is a likely explanation for the null result in contrast to MTsat.[22] T1 prolongation, which accompanies increased myelin damage,[65] may systematically affect MTR in such a way as to render it less sensitive to demyelination than MTsat, since MTsat disentangles T1 relaxation effects from MT.[22] Indeed, the longitudinal decline in NAWM MTR has been estimated at 0.1% per year,[66] and previous case-control studies show that MTR in NAWM is typically only 1.25 percent units lower than control white matter, reiterating the subtlety of NAWM changes.[21] Longer follow-up may therefore be required in order to detect changes in NAWM MTR in early RRMS.

In our cohort of patients with recently diagnosed RRMS, we observed an unexpected increase in NODDI ICVF within NAWM over one year. NODDI ICVF represents the 'restricted' diffusion signal fraction within the non-isotropic diffusion signal; ICVF is typically lower in RRMS compared to healthy controls[28,60,67] and longitudinal decreases in NAWM ICVF have previously been noted.[68] The biological mechanism driving the increase in NODDI ICVF, with no concomitant change in ISOVF, is unclear, but could partly be attributed to axonal swelling, axonal bundling following demyelination, or axonal repair. Axonal regeneration *per se* appears unlikely given the limited ability of the CNS to repair following axonal injury,[69] and the lack of positive association with change in whole brain volume, an established marker of neurodegeneration. A decrease in glial cell infiltration following resolution of acute inflammation could also explain an increase in ICVF relative to a resulting decrease in hindered diffusion.

The observed absence of longitudinal change in NODDI ISOVF was expected as significant increases in water content would likely be visible as hyperintense signal on conventional T2 FLAIR, and thus classified as lesions.

The longitudinal increase in g-ratio within NAWM observed in patients with recently diagnosed RRMS is consistent with subtle demyelination in early RRMS which is not otherwise visible on conventional MRI. The MR g-ratio has been applied in cross-sectional studies of MS,[30,34,70,71] healthy cohorts,[72] other diseases (e.g. Moyamoya disease[73], Huntington's disease[74]), and childhood development,[75] yet longitudinal analysis of g-ratio in the adult brain has been notably lacking. Our results illustrate that g-ratio may be suited to assessing myelin integrity changes over time. Conversely, an increase in g-ratio could also result from the observed increase in NODDI ICVF. Nevertheless, the strong relationship in NAWM between longitudinal change in g-ratio and MTsat but little association with NODDI measures suggests that myelin loss is driving the longitudinal increase in NAWM g-ratio.

Similarly to MTsat, the majority of patient data points for g-ratio in NAWM fell within limits of agreement established from healthy control test-retest measures. While the significant group-wise longitudinal change in g-ratio indicates a biological change in NAWM over one year post-diagnosis in RRMS, such change may not exceed measurement error for an individual patient.

White matter lesions

In WMLs, MTsat increased over one year, suggestive of myelin repair, but MTR did not change after accounting for covariates, indicating that MTsat may be more sensitive to alterations in myelin integrity, including spontaneous remyelination. To date, no other studies to our knowledge have examined longitudinal evolution of MTsat in MS lesions; MTR, on the other hand, may fluctuate with time and lesion type (e.g. contrast-enhancing versus non-enhancing lesions).[21] While we did not investigate lesion sub-types in this study, the discrepancy between MTsat and MTR results suggests that T1 effects may be a contributing factor. Although a decrease in water content could account for a lesion-specific increase in MTsat, the increase in NODDI ISOVF within lesions suggests this is not the case. Moreover, the effect size was large with several patients exceeding limits of agreement established in control

white matter. As such, some recovery of myelin following acute inflammation appears to be a plausible explanation.

Early treatment with DMTs, which target inflammation and reduce likelihood of progression,[10] could also contribute to the increase in lesion MTsat. All patients in our cohort were treatment-naïve at baseline but nearly two thirds of patients had commenced DMTs by one year follow-up. Initiation of DMTs was not a significant covariate in WML models, however, suggesting that spontaneous remyelination may be a more significant effect. MTsat within lesions did not reach NAWM levels, demonstrating that any remyelination is patchy. Another possible explanation is reclassification of NAWM tissue as WMLs over time; new or enlarging lesions may not be as extensively damaged and thus could explain increases in MT within lesions.

The increase in NODDI ICVF within cerebral WML was greater than in NAWM and exceeded limits of agreement from healthy controls, although WML ICVF remained lower than in NAWM. Again, this unexpected increase in NODDI ICVF within WML may be explained by a post-relapse reduction in glial cell presence, or poor adaptability of the NODDI model to pathological tissue. Again, axonal recovery seems an unlikely explanation, although NODDI ICVF could also be sensitive to myelin status and hence remyelination.

The increase in NODDI ISOVF within WMLs over one year, indicating greater isotropic diffusion, does however suggest ongoing progressive destruction of neuroaxonal architecture. Together, these results could reflect heterogeneous tissue repair within lesions. This is further supported by the lack of relationship between NODDI metrics (Supplementary Figure 8F) and weak negative relationship between change in MTsat and NODDI ISOVF in WMLs (Supplementary Figure 8E).

G-ratio, an aggregate of MT and dMRI measure, did not change in WMLs over one year. The lack of change in g-ratio within WMLs may be due to competing effects; significant increases in NODDI ICVF and NODDI ISO in parallel with increases in MTsat, suggestive of remyelination, oppose each other to some degree (see Supplementary Figure 3). Intra-patient heterogeneity across lesions may also explain the negative result, and g-ratio changes on a lesion-by-lesion basis cannot be ruled out.

Further investigation showed that, in spite of a strong correlation between changes in MTsat and g-ratio in NAWM, the relationship between longitudinal changes in MTsat and g-ratio is weaker in WMLs. This highlights the importance of considering both diffusion metrics and myelin-sensitive imaging markers when tracking heterogeneous pathology in RRMS. While MTsat may be sensitive to myelinated axonal integrity, there may be a “floor” effect in focal areas of low myelin density which may limit the usefulness of the MTsat signal within WMLs.

Implications of findings

Through the incorporation of simulations, healthy control data and longitudinal data from a sizable patient cohort, this study unpicks the sensitivity of MTI and dMRI-NODDI metrics to early pathological processes in RRMS, within NAWM and WML. We demonstrate that MTsat is well-suited to subtle demyelination whilst NODDI measures may be adept to WML. Combining the MTI and dMRI through the MR g-ratio may be useful for studying NAWM, however interpretation of longitudinal change is complex; the g-ratio model may therefore not be optimal for WML.

Limitations

There are a number of limitations in the present study. NODDI, MTsat and g-ratio analyses are heavily model-dependent and based on assumptions from healthy brain tissue, some of which may break down where there is marked loss of normal microstructural integrity. Of note, g-ratio maps here were calibrated from healthy control data; there was no validation of this calibration in non-MR histological data, and the model assumes a g-ratio of 0.7 in the splenium of the corpus callosum as a prior, which may be flawed. Moreover, T1app provides an approximation of T1 recovery and may not be as accurate as T1 derived from quantitative compartmental modelling of the MT signal. T1app does, however, allow disentanglement of T1 recovery effects in our MTI metric, MTsat. Finally, limits of agreement were established in healthy control white matter and may not apply for WML; yet assessment of test-retest agreement is an important step performed in our study to establish sensitivity to detection of pathological change.

The cohort itself is limited by the short follow-up duration. RRMS is inherently a disease that undergoes periods of worsening and stable disease. Over one year, therefore, a substantial number of patients will be recovering from an acute

inflammatory episode and there will be limited opportunity to capture divergence of disease progression. Nevertheless the incorporation of longitudinal data from a sizable cohort of people who were recruited at a similar disease stage is a strength of this study.

Finally, loss of subject data to drop-out and technical inaccuracies may introduce bias to the analyses, and longitudinal biological change may not exceed expected measurement error in an individual patient.

Conclusion

MTsat and MRI g-ratio, derived from NODDI and MTsat data, are promising *in vivo* biomarkers of myelin integrity. MTsat is more sensitive than MTR for detecting loss of NAWM myelin integrity in early RRMS. Longitudinal increases in MTsat and NODDI metrics in WMLs suggest recovery from a neuroinflammatory episode following diagnosis of RRMS.

Our findings suggest that the most sensitive and useful microstructural measures depend on the degree of tissue damage; MTsat and g-ratio detect subtle change in NAWM, whereas T1 recovery and NODDI parameters are more suited to evaluating severely damaged WML. Although the g-ratio has a specific histopathological correlate with myelin thickness in tissue, simulations and empirically-determined distributions of microstructural metrics demonstrate that biological interpretation of g-ratio in isolation is complex in the presence of changes in NODDI parameters. Independent consideration of myelin-sensitive and axonal neuroimaging markers may ultimately be more informative for longitudinal tracking of neuropathology in RRMS than combining such measures. Technique reproducibility, however, currently limits sensitivity to pathological change in individual patients.

Further research is required to broaden the applicability of diffusion and MT models, and validate these against tissue measures across the heterogeneous tissue damage found in MS, for application in clinical practice and therapeutic trials.

Acknowledgements

With special thanks to all participants in FutureMS and the radiographers at the RIE Edinburgh. We would also like to thank other non-author contributors of the

FutureMS consortium as follows: Chris Batchelor, Emily Beswick, Fraser Brown, Tracy Brunton, Jessie Chang, Yingdi Chen, Shuna Colville, Peter Connick, Annette Cooper, Denise Cranley, Rachel Dakin, Baljean Dhillon, Liz Elliott, Peter Foley, Stella Glasmacher, Angus Grossart, Haane Haagenrud, Katarzyna Hafezi, Emily Harrison, Sara Hathorn, David Hunt, Aidan Hutchison, Charlotte Jardine, Kiran Jayprakash, Matt Justin, Patrick Kearns, Lucy Kessler, Michaela Kleynhans, Juan Larraz, Dawn Lyle, Niall MacDougall, Jen MacFarlane, Alan Maclean, Bev MacLennan, Nicola Macleod, Don Mahad, Sarah-Jane Martin, Daisy Mollison, Mary Monaghan, Lee Murphy, Katy Murray, Judith Newton, Julian Ng Kee Kwong, David Perry, Suzanne Quigley, Scott Semple, Adam Scotson, Amy Stenson, Maria Valdez Hernandez, Christine Weaver, Belinda Weller, Anna Williams, Stewart Wiseman, Charis Wong, Michael Wong and Rosie Woodward

Funding Sources

ENY was supported by a Chief Scientist Office SPRINT MND/MS Studentship and funding from the Anne Rowling Regenerative Neurology Clinic, Edinburgh. MJT is funded by the NHS Lothian Research and Development Office. RM and AK are funded by the UK MS Society Edinburgh Centre for MS Research grant (grant reference 133). FutureMS, hosted by Precision Medicine Scotland Innovation Centre (PMS-IC), was funded by a grant from the Scottish Funding Council to PMS-IC and Biogen Idec Ltd Insurance. Additional funding for the University of Edinburgh 3T MRI Research scanner in Royal Infirmary Edinburgh is funded by Wellcome (104916), Dunhill Trust (R380R/1114), Edinburgh and Lothians Health Foundation (2012/17), Muir Maxwell Research Fund, Edinburgh Imaging, and University of Edinburgh.

Competing interests

The authors declare no conflicts of interests.

References

1. Bitsch A, Schuchardt J, Bunkowski S, Kuhlmann T, Bruck W. Acute axonal injury in multiple sclerosis: Correlation with demyelination and inflammation. *Brain.* 2000;123(6):1174-1183.
2. Lassmann H. Multiple Sclerosis Pathology. *Cold Spring Harb Perspect Med.* 2018;8(3).
3. Charcot JM. *Histologie de la sclérose en plaques.* Paris1868.
4. Frischer JM, Bramow S, Dal-Bianco A, et al. The relation between inflammation and neurodegeneration in multiple sclerosis brains. *Brain.* 2009;132(Pt 5):1175-1189.
5. MS Society. Definition of MS. https://www.nationalmssociety.org/What-is-MS/Definition-of-MS. Accessed 21 June 2019.
6. Brownlee WJ, Hardy TA, Fazekas F, Miller DH. Diagnosis of multiple sclerosis: progress and challenges. *The Lancet.* 2017;389(10076):1336-1346.
7. Gelfand JM. Multiple sclerosis: diagnosis, differential diagnosis, and clinical presentation. *Handb Clin Neurol.* 2014;122:269-290.
8. Filippi M, Bar-Or A, Piehl F, et al. Multiple sclerosis. *Nat Rev Dis Primers.* 2018;4(1):43.
9. Lorscheider J, Buzzard K, Jokubaitis V, et al. Defining secondary progressive multiple sclerosis. *Brain.* 2016;139(Pt 9):2395-2405.
10. Brown JWL, Coles A, Horakova D, et al. Association of Initial Disease-Modifying Therapy With Later Conversion to Secondary Progressive Multiple Sclerosis. *JAMA.* 2019;321(2):175-187.
11. Scalfari A, Neuhaus A, Degenhardt A, et al. The natural history of multiple sclerosis: a geographically based study 10: relapses and long-term disability. *Brain.* 2010;133(Pt 7):1914-1929.
12. Barkhof F. The clinico-radiological paradox in multiple sclerosis revisited. *Curr Opin Neurol.* 2002;15(3):239-245.
13. Sati P, Oh J, Constable RT, et al. The central vein sign and its clinical evaluation for the diagnosis of multiple sclerosis: a consensus statement from the North American Imaging in Multiple Sclerosis Cooperative. *Nat Rev Neurol.* 2016;12(12):714-722.
14. Rindfleisch E. Histologisches Detail zu der grauen Degeneration von Gehirn und Rückenmark. (Zugleich ein Beitrag zu der Lehre von der Entstehung und Verwandlung der Zelle.). *Archiv für Pathologische Anatomie und Physiologie und für Klinische Medicin.* 1863;26(5-6):474-483.
15. Rae-Grant AD, Wong C, Bernatowicz R, Fox RJ. Observations on the brain vasculature in multiple sclerosis: A historical perspective. *Mult Scler Relat Disord.* 2014;3(2):156-162.
16. Putnam TJ. The Pathogenesis of Multiple Sclerosis: A Possible Vascular Factor. *New England Journal of Medicine.* 1933;209(16):786-790.

17. Wattjes MP, Ciccarelli O, Reich DS, et al. 2021 MAGNIMS–CMSC–NAIMS consensus recommendations on the use of MRI in patients with multiple sclerosis. *The Lancet Neurology.* 2021;20(8):653-670.

18. Zeis T, Graumann U, Reynolds R, Schaeren-Wiemers N. Normal-appearing white matter in multiple sclerosis is in a subtle balance between inflammation and neuroprotection. *Brain.* 2008;131(Pt 1):288-303.

19. Kutzelnigg A, Lucchinetti CF, Stadelmann C, et al. Cortical demyelination and diffuse white matter injury in multiple sclerosis. *Brain.* 2005;128(Pt 11):2705-2712.

20. Allen IV, McKeown SR. A histological, histochemical and biochemical study of the macroscopically normal white matter in multiple sclerosis. *Journal of the Neurological Sciences.* 1979;41(1):81-91.

21. York EN, Thrippleton MJ, Meijboom R, Hunt DPJ, Waldman AD. Quantitative magnetisation transfer imaging in relapsing-remitting multiple sclerosis: a systematic review and meta-analysis. (pre-print, accepted in Brain Communications). *medRxiv.* 2021.

22. Helms G, Dathe H, Kallenberg K, Dechent P. High-resolution maps of magnetization transfer with inherent correction for RF inhomogeneity and T1 relaxation obtained from 3D FLASH MRI. *Magnetic Resonance in Medicine.* 2008;60(6):1396-1407.

23. Yi SY, Barnett BR, Torres-Velazquez M, et al. Detecting Microglial Density With Quantitative Multi-Compartment Diffusion MRI. *Front Neurosci.* 2019;13:81.

24. Jones DK, Knosche TR, Turner R. White matter integrity, fiber count, and other fallacies: the do's and don'ts of diffusion MRI. *Neuroimage.* 2013;73:239-254.

25. Zhang H, Schneider T, Wheeler-Kingshott CA, Alexander DC. NODDI: practical in vivo neurite orientation dispersion and density imaging of the human brain. *Neuroimage.* 2012;61(4):1000-1016.

26. Hagiwara A, Kamagata K, Shimoji K, et al. White Matter Abnormalities in Multiple Sclerosis Evaluated by Quantitative Synthetic MRI, Diffusion Tensor Imaging, and Neurite Orientation Dispersion and Density Imaging. *AJNR Am J Neuroradiol.* 2019;40(10):1642-1648.

27. Rahmanzadeh R, Lu PJ, Barakovic M, et al. Myelin and axon pathology in multiple sclerosis assessed by myelin water and multi-shell diffusion imaging. *Brain.* 2021;144(6):1684-1696.

28. Alotaibi A, Podlasek A, AlTokhis A, Aldhebaib A, Dineen RA, Constantinescu CS. Investigating Microstructural Changes in White Matter in Multiple Sclerosis: A Systematic Review and Meta-Analysis of Neurite Orientation Dispersion and Density Imaging. *Brain Sci.* 2021;11(9).

29. Stikov N, Campbell JS, Stroh T, et al. In vivo histology of the myelin g-ratio with magnetic resonance imaging. *Neuroimage.* 2015;118:397-405.

30. York EN, Martin SJ, Meijboom R, et al. MRI-derived g-ratio and lesion severity in newly diagnosed multiple sclerosis. *Brain Commun.* 2021;3(4):fcab249.

31. Rushton WA. A theory of the effects of fibre size in medullated nerve. *J Physiol.* 1951;115(1):101-122.

32. Chomiak T, Hu B. What is the optimal value of the g-ratio for myelinated fibers in the rat CNS? A theoretical approach. *PLoS One.* 2009;4(11):e7754.

33. Ellerbrock I, Mohammadi S. Four in vivo g-ratio-weighted imaging methods: Comparability and repeatability at the group level. *Hum Brain Mapp.* 2018;39(1):24-41.

34. Kamagata K, Zalesky A, Yokoyama K, et al. MR g-ratio-weighted connectome analysis in patients with multiple sclerosis. *Sci Rep.* 2019;9:13.

35. Campbell JSW, Leppert IR, Narayanan S, et al. Promise and pitfalls of g-ratio estimation with MRI. *Neuroimage.* 2018;182:80-96.

36. Hori M, Hagiwara A, Fukunaga I, et al. Application of Quantitative Microstructural MR Imaging with Atlas-based Analysis for the Spinal Cord in Cervical Spondylotic Myelopathy. *Sci Rep.* 2018;8(1):5213.

37. Mohammadi S, Callaghan MF. Towards in vivo g-ratio mapping using MRI: Unifying myelin and diffusion imaging. *J Neurosci Methods.* 2021;348:108990.

38. Meijboom R, Wiseman SJ, York EN, et al. Rationale and design of the brain magnetic resonance imaging protocol for FutureMS: a longitudinal multi-centre study of newly diagnosed patients with relapsing-remitting multiple sclerosis in Scotland. *Wellcome Open Research.* 2022.

39. Polman CH, Reingold SC, Banwell B, et al. Diagnostic criteria for multiple sclerosis: 2010 revisions to the McDonald criteria. *Ann Neurol.* 2011;69(2):292-302.

40. Li X, Morgan PS, Ashburner J, Smith J, Rorden C. The first step for neuroimaging data analysis: DICOM to NIfTI conversion. *J Neurosci Methods.* 2016;264:47-56.

41. Meijboom R, Wiseman SJ, York EN, et al. Rationale and design of the brain magnetic resonance imaging protocol for FutureMS: a longitudinal multi-centre study of newly diagnosed patients with relapsing-remitting multiple sclerosis in Scotland. *medRxiv.* 2021.

42. York ET, Michael J; Waldman, Adam. Magnetisation transfer saturation (MTsat) processing. In. University of Edinburgh. Centre for Clinical Brain Sciences.2020.

43. Helms G, Hagberg GE. In vivo quantification of the bound pool T1 in human white matter using the binary spin-bath model of progressive magnetization transfer saturation. *Physics in medicine and biology.* 2009;54(23):N529-540.

44. Jenkinson M, Bannister P, Brady M, Smith S. Improved Optimization for the Robust and Accurate Linear Registration and Motion Correction of Brain Images. *NeuroImage.* 2002;17(2):825-841.

45. Jenkinson M, Smith S. A global optimisation method for robust affine registration of brain images. *Medical Image Analysis.* 2001;5(2):143-156.

46. Helms G, Dathe H, Dechent P. Erratum to Helms, Dathe, and Dechent. Quantitative FLASH MRI at 3 tesla using a rational approximation of the ernst

equation. Magn Reson Med 2008;59:667-672. *Magnetic Resonance in Medicine.* 2010;63(4):1136-1136.

47. Helms G, Dathe H, Dechent P. Quantitative FLASH MRI at 3T using a rational approximation of the Ernst equation. *Magnetic Resonance in Medicine.* 2008;59(3):667-672.

48. Martin Bland J, Altman D. Statistical Methods for Assessing Agreement between Two Methods of Clinical Measurement. *The Lancet.* 1986;327(8476):307-310.

49. Bates D, Mächler M, Bolker B, Walker S. Fitting Linear Mixed-Effects Models Usinglme4. *Journal of Statistical Software.* 2015;67(1).

50. Kuznetsova A, Brockhoff PB, Christensen RHB. lmerTest Package: Tests in Linear Mixed Effects Models. *Journal of Statistical Software.* 2017;82(13).

51. Nakagawa S, Johnson PCD, Schielzeth H. The coefficient of determination R(2) and intra-class correlation coefficient from generalized linear mixed-effects models revisited and expanded. *J R Soc Interface.* 2017;14(134).

52. Lüdecke D, Ben-Shachar M, Patil I, Waggoner P, Makowski D. performance: An R Package for Assessment, Comparison and Testing of Statistical Models. *Journal of Open Source Software.* 2021;6(60).

53. Field AS, Samsonov A, Alexander AL, Mossahebi P, Duncan ID. Conventional and quantitative MRI in a novel feline model of demyelination and endogenous remyelination. *J Magn Reson Imaging.* 2019;49(5):1304-1311.

54. Gringel T, Schulz-Schaeffer W, Elolf E, Frolich A, Dechent P, Helms G. Optimized high-resolution mapping of magnetization transfer (MT) at 3 Tesla for direct visualization of substructures of the human thalamus in clinically feasible measurement time. *J Magn Reson Imaging.* 2009;29(6):1285-1292.

55. Lema A, Bishop C, Malik O, et al. A Comparison of Magnetization Transfer Methods to Assess Brain and Cervical Cord Microstructure in Multiple Sclerosis. *J Neuroimaging.* 2017;27(2):221-226.

56. Helms G, Dathe H, Dechent P. Modeling the influence of TR and excitation flip angle on the magnetization transfer ratio (MTR) in human brain obtained from 3D spoiled gradient echo MRI. *Magn Reson Med.* 2010;64(1):177-185.

57. Levesque I, Sled JG, Narayanan S, et al. The role of edema and demyelination in chronic T1 black holes: a quantitative magnetization transfer study. *J Magn Reson Imaging.* 2005;21(2):103-110.

58. Vavasour IM, Li DK, Laule C, Traboulsee AL, Moore GR, Mackay AL. Multi-parametric MR assessment of T(1) black holes in multiple sclerosis : evidence that myelin loss is not greater in hypointense versus isointense T(1) lesions. *J Neurol.* 2007;254(12):1653-1659.

59. Grussu F, Schneider T, Tur C, et al. Neurite dispersion: a new marker of multiple sclerosis spinal cord pathology? *Ann Clin Transl Neurol.* 2017;4(9):663-679.

60. Johnson D, Ricciardi A, Brownlee W, et al. Comparison of Neurite Orientation Dispersion and Density Imaging and Two-Compartment Spherical Mean

Technique Parameter Maps in Multiple Sclerosis. *Front Neurol.* 2021;12:662855.

61. Chung AW, Seunarine KK, Clark CA. NODDI reproducibility and variability with magnetic field strength: A comparison between 1.5 T and 3 T. *Hum Brain Mapp.* 2016;37(12):4550-4565.

62. Andica C, Kamagata K, Hayashi T, et al. Scan-rescan and inter-vendor reproducibility of neurite orientation dispersion and density imaging metrics. *Neuroradiology.* 2020;62(4):483-494.

63. Gong T, Tong Q, He H, Sun Y, Zhong J, Zhang H. MTE-NODDI: Multi-TE NODDI for disentangling non-T2-weighted signal fractions from compartment-specific T2 relaxation times. *Neuroimage.* 2020;217:116906.

64. Lommers E, Simon J, Reuter G, et al. Multiparameter MRI quantification of microstructural tissue alterations in multiple sclerosis. *Neuroimage Clin.* 2019;23:101879.

65. Al-Radaideh A, Mougin OE, Lim SY, Chou IJ, Constantinescu CS, Gowland P. Histogram analysis of quantitative T1 and MT maps from ultrahigh field MRI in clinically isolated syndrome and relapsing-remitting multiple sclerosis. *NMR Biomed.* 2015;28(11):1374-1382.

66. Davies GR, Altmann DR, Hadjiprocopis A, et al. Increasing normal-appearing grey and white matter magnetisation transfer ratio abnormality in early relapsing-remitting multiple sclerosis. *J Neurol.* 2005;252(9):1037-1044.

67. Collorone S, Cawley N, Grussu F, et al. Reduced neurite density in the brain and cervical spinal cord in relapsing-remitting multiple sclerosis: A NODDI study. *Mult Scler.* 2020;26(13):1647-1657.

68. Sacco S, Caverzasi E, Papinutto N, et al. Neurite Orientation Dispersion and Density Imaging for Assessing Acute Inflammation and Lesion Evolution in MS. *AJNR Am J Neuroradiol.* 2020;41(12):2219-2226.

69. Huebner EA, Strittmatter SM. Axon regeneration in the peripheral and central nervous systems. *Results Probl Cell Differ.* 2009;48:339-351.

70. Yu F, Fan Q, Tian Q, et al. Imaging G-Ratio in Multiple Sclerosis Using High-Gradient Diffusion MRI and Macromolecular Tissue Volume. *AJNR Am J Neuroradiol.* 2019;40(11):1871-1877.

71. Maekawa T, Hagiwara A, Yokoyama K, et al. Multiple sclerosis plaques may undergo continuous myelin degradation: a cross-sectional study with myelin and axon-related quantitative magnetic resonance imaging metrics. *Neuroradiology.* 2022;64(3):465-471.

72. Mohammadi S, Carey D, Dick F, et al. Whole-Brain In-vivo Measurements of the Axonal G-Ratio in a Group of 37 Healthy Volunteers. *Front Neurosci.* 2015;9:441.

73. Hara S, Hori M, Hagiwara A, et al. Myelin and Axonal Damage in Normal-Appearing White Matter in Patients with Moyamoya Disease. *AJNR Am J Neuroradiol.* 2020;41(9):1618-1624.

74. Johnson EB, Parker CS, Scahill RI, et al. Altered iron and myelin in premanifest Huntington's Disease more than 20 years before clinical onset:

Evidence from the cross-sectional HD Young Adult Study. *EBioMedicine.* 2021;65:103266.

75. Geeraert BL, Lebel RM, Lebel C. A multiparametric analysis of white matter maturation during late childhood and adolescence. *Hum Brain Mapp.* 2019;40(15):4345-4356.